THREE-DIMENSIONAL INVERSION OF AIRBORNE ZTEM AND AIRMT DATA

by

Muran Han

A thesis submitted to the faculty of
The University of Utah
in partial fulfillment of the requirements for the degree of

Master of Science

in

Geophysics

Department of Geology and Geophysics

The University of Utah

December 2017

The University of Utah Graduate School

STATEMENT OF THESIS APPROVAL

The thesis of **Muran Han**

has been approved by the following supervisory committee members:

Michael S. Zhdanov	, Chair	**03/23/2017** Date Approved
Erich U. Petersen	, Member	**10/07/2013** Date Approved
Alexander V. Gribenko	, Member	**09/11/2013** Date Approved

and by **Thure E. Cerling** , Chair of the Department of **Geology and Geophysics**

and by David B. Kieda, Dean of The Graduate School.

ABSTRACT

In this thesis, an interpretation technique is developed and presented for two new airborne geophysical methods which are used for measuring natural magnetic fields: ZTEM and AirMt. The z-axis tipper electromagnetic (ZTEM) system measures the fields of natural audio-frequency sources using an airborne vertical magnetic field receiver and a pair of horizontal, magnetic field ground receivers at a base station. The AirMt method employs three orthogonal airborne magnetic field receivers and three horizontal orthogonal magnetic-field ground receivers at a base station. The magnetic field components acquired during the AirMt survey are converted into an amplification parameter, which is invariant to receiver reference systems. The airborne deployment makes it possible to acquire ZTEM and AirMt data over large areas for a relatively low cost compared to equivalent ground surveys. This makes it a practical method for mapping large-scale geological structures. This thesis develops the methods of three-dimensional (3D) forward modeling and inversion of ZTEM and AirMt data. For the forward modeling, I apply the integral equation method, while the inversion is based on Tikhonov regularization method. The model study in this thesis is conducted under different conditions which can affect accurate modeling and inversion of the data. In the final chapter of the thesis, I present the results of inversion of the field ZTEM data from the Cochrane test site in Ontario, Canada.

To my parents and my wife, Xiao

TABLE OF CONTENTS

ACKNOWLEDGMENTS

Before I joined the Consortium for Electromagnetic Modeling and Inversion (CEMI) at the Department of Geology and Geophysics, University of Utah, I didn't have much knowledge about electromagenetic methods, especially of forward modeling and inversion, which requires good math skills. There are too many people to thank. Therefore, I will be lengthy here and brief elsewhere.

I am deeply indebted to my advisor and committee chair, Dr. Michael Zhdanov, who made this work possible and shared his vast knowledge of EM and inversion, for giving me a chance to work under his guidance and for ultimately leading me along an academic path. Dr. Le Wan not only sacrificed a lot of time to explain the problems of EM theory to me, but also made many invaluable insights into the application of my research in the real world and forced me to look beyond my work. Dr. Alexander V. Gribenko, who is an EM expert in my mind, provided helpful guidance for this work and answered numerous questions about programming and inversion techniques.

I would also like to thank my advisor, Dr. Erich Petersen, who guided me to connect geophysics with geology, especially when it comes to minerals and rocks.

I also thank Dr. Martin Cuma and Dr. Xiaojun Liu for sharing the techniques and skills of parallel computation, discussing things related to my thesis research, addressing questions related to practical geophysical situations, and providing invaluable codes to refer to for this research. I also thank Mrs. Kim Atwater. Without her help, I would have a

lot of trouble in life.

Finally, my family provided empathy and encouragement along the way. I especially thank my parents. Without their encouragement and help, I could not have focused on my work completely. Most of all, I would like to thank my wife, Xiao, for supporting my study, which was a long journey from beginning to the end。

CHAPTER 1

INTRODUCTION

ZTEM is a novel electromagnetic (EM) geophysical technique used in measuring the natural magnetic field, similar to magnetotelluric (MT) methods and coupled with rapid spatial acquisition from an airborne system. In understanding the electrical conductivity of the upper regions of the earth, the MT method plays a very important role. The primary advantage of natural source EM, especially the airborne method, compared with the controlled source method, is the large depth of penetration due to the relatively low frequencies used. Particularly, the MT method plays a significant role in crustal studies as well as in hydrocarbon and mineral exploration. However, the MT technique and other deep-probing controlled source EM methods have some obvious practical limitations, related to the cost of the survey and the time required for the data acquisition. Measuring the MT field from an airborne platform is very attractive, because it allows us to cover large areas very quickly and it does not require using a controlled source. The main problem with the airborne implementation of the MT method is related to the fact that the airborne measurement of an electric field is extremely difficult; therefore, the airborne method should be based on magnetic data only. It has long been recognized that tipper data, the ratio of the local vertical magnetic field to the horizontal magnetic field, provide information about the anomalies of the three-dimensional (3D) electrical conductivity. The

fundamental reason for this is that the inducing electromagnetic fields are vertically propagating plane waves, so if the earth is one-dimensional (1D), the vertical component of the magnetic field will be zero. Nonzero values of the tipper data are directly related to anomalous currents. It was this understanding that prompted the development of the audio frequency magnetics (AFMAG) technique (Ward, 1959). The original airborne AFMAG technique used the amplitude outputs from two orthogonal coils towed behind an aircraft to determine the tilt of the plane and the polarization of the natural magnetic field.

To improve the AFMAG method, Labson and others (1985) developed a technique that used ground-based horizontal and vertical coils to measure the reference magnetic fields. They used MT processing techniques to show how tipper data could be obtained from the measured magnetic fields.

A further improvement to the original AFMAG technique combines improved instrumentation and MT data processing techniques. This has resulted in the z-axis tipper electromagnetic method (ZTEM) (Lo and Zang, 2008). In this method, the vertical component of the magnetic field is recorded over the entire survey area, while the horizontal fields are recorded at a ground-based reference station (Holtham and Oldenburg, 2010). The MT processing technique produces the frequency domain transfer functions that relate the vertical fields over the survey area to the horizontal fields at the reference station. By taking ratios of the two fields (similar to taking ratios of the E and H fields in MT), the effect of the unknown source function is removed. Since new instrumentation exists to measure the vertical magnetic fields by helicopter, the magnetic data over large survey areas can quickly be collected. The result is a cost-effective procedure for collecting natural source EM data that provide information about the 3D conductivity structure of the

earth. Over the last several years, industry has recognized the potential of this technique and the need to be able to invert these data (Zhdanov and Golubev, 2003).

Another airborne MT method considered in this thesis is called AirMt (Gribenko et al., 2012). In general, the 3D magnetic field variations measured at the airborne receiver platform are related to the horizontal incident fields at a base station by an AirMt tensor. The AirMt system measures the magnetic field within some frequency bands at the base station and from the airborne system. Using these measurements, one can derive the components of the AirMt tensor. The compact amplification parameter P is further established as a function of the cross product of the two columns of the AirMt tensor. It can be shown that parameter P is invariant under any rotation of the airborne frame of reference or the base station frame of reference, thus making AirMt measurements immune to tilt errors (Kuzmin et al., 2010).

Zhdanov et al. (2011) presented an inversion algorithm for both individual ZTEM data and for joint MT and ZTEM data. In this thesis, a 3D AirMT data inversion capability is developed, extending the two-dimensional (2D) expressions of the AirMT Fréchet derivative presented by Wannamaker (1984) to a 3D case.

I have also developed a 3D inversion algorithm for ZTEM and AirMt data. Forward modeling is fundamental to any inversion algorithm, and a simple forward model was used to produce the results of the ZTEM and AirMt data. Next, algorithms were developed for inverting ZTEM and AirMt data. Finally, the output data of the forward modeling were used as the input for the ZTEM and AirMt inversion to invert the model data, and both inversions were compared with each other to test the program. Synthetic modeling is used to study the effects of background conductivity variations, different flight elevations, and

noise for both ZTEM and AirMt inversions. The results of 3D ZTEM data inversion over the Cochrane test site in Ontario, Canada, and the effectiveness of developed methods and codes is demonstrated and presented in this thesis as well.

CHAPTER 2

FOUNDATIONS OF THE AIRBORNE MAGNETOVARIATIONAL METHODS

Long-term observations show that the magnitude and direction of the earth's magnetic field continuously change with time. These alterations are called *geomagnetic variations*. There are two types of geomagnetic variations: one is caused by internal sources while the other one is due to an external origin (Campbell, 2003).

According to electromagnetic induction laws, geomagnetic variations induce a transient electromagnetic field in the conductive earth, and the corresponding electric current. Note that the external geomagnetic variations vary rapidly and can induce a strong current, which is easy to measure. This current is called a *telluric current* (from the Latin word *telluric* for earth's). As a result, the entire field of geomagnetic variations and telluric currents is called the *magnetotelluric field* (Zhdanov, 2009) .

The magnetotelluric field at frequencies below 1 hertz is of particular importance, primarily because it can be used as an energy source to probe the earth to great depths. At these low frequencies, the magnetotelluric field originates almost entirely from complex interactions between the earth's magnetosphere and the flow of plasma from the sun (solar wind) (Zhdanov, 2009).

In this chapter, the concept of transfer functions will be considered, and the

principles of the two different airborne EM methods, ZTEM and AirMt, will be discussed.

2.1 Magnetic transfer functions

Variations of the natural MT field can be separated into two parts: telluric (electric) and geomagnetic (magnetic) variations. These variations are caused by ionospheric and magnetospheric currents arising from interactions between the solar and a magnetosphere plasma with a constant geomagnetic field (Berdichevskii and Dmitriev, 2008). Practical MT data are observed over a range of periods from a fraction of a second to several hours. Such fields can penetrate into the earth at a depth from several hundred meters to several hundred kilometers, which is of great importance to the study of the geoelectrical structure of the earth's deep interior.

The intensity of the natural source in the MT method is unknown. In order to eliminate this source effect, scientists study the ratio of the electric and magnetic fields, which is defined as the impedance, rather than the natural electromagnetic field itself. The concept of impedance (Cagniard, 1953; Tikhonov, 1950) helps to build the fundamental principles of magnetotellurics and makes the MT method a powerful tool to study the geoelectrical structure of the earth.

The expression for impedance is misleadingly simple:

$$Z = E_x/H_y = -E_y/H_x, \tag{2.1}$$

where $\{E_x, E_y\}$ and $\{H_x, H_y\}$ represent the horizontal components of the electric and magnetic fields. We assume a linearity in the relationships between the mutually orthogonal electric and magnetic field components which are used in determining the Tikhonov-Cagniard impedance:

$$E_x = ZH_y,$$

$$E_y = -ZH_x\ . \tag{2.2}$$

It is most important to consider the question of the validity of this assumption of linearity when we are dealing with a real, inhomogeneous earth. The answer to this question rests on a detailed analysis of the linearity between the various components of the magnetotelluric field. We will make this analysis using some elementary concepts of linear algebra.

In a general case, a monochromatic field satisfies the following equations:

$$\mathrm{curl}\vec{H} = \sigma\vec{E} + \overrightarrow{j^Q},$$

$$\mathrm{curl}\vec{E} = i\omega\mu_0\vec{H}, \tag{2.3}$$

where $\overrightarrow{j^Q}$ is the volume density of the external ionospheric and magnetospheric currents which give rise to the magnetotelluric field. On the strength of Maxwell's equations being linear, it is possible to write the electric and magnetic fields as linear transformations of the current density vector $\overrightarrow{j^Q}$:

$$\vec{E}(r) = \iiint_Q \widehat{G}^E\left(\vec{r}\middle|\overrightarrow{r'},\omega,\sigma\right)\overrightarrow{j^Q}\left(\overrightarrow{r'}\right)dv',$$

$$\vec{H}(r) = \iiint_Q \widehat{G}^H\left(\vec{r}\middle|\overrightarrow{r'},\omega,\sigma\right)\overrightarrow{j^Q}\left(\overrightarrow{r'}\right)dv', \tag{2.4}$$

where Q is the region within which the currents $\overrightarrow{j^Q}$ are present, and $\widehat{G}^E$ and $\widehat{G}^H$are linear operators related to the radius vector $\vec{r}$ defining the location at which the field is observed and the radius vectors $\overrightarrow{r'}$ defining the points at which the source currents $\overrightarrow{j^Q}\left(\overrightarrow{r'}\right)$ are flowing. These operators are functions only of the field frequency ω and the distribution of electrical conductivity in the medium, σ. A prime indicates that integration has been

carried out with respect to $\vec{r'}$.

In the theory of linear relationships between the components of magnetotelluric fields (Zhdanov, 2009), it has been shown that for most types of geomagnetic variations (pulsations, microstorms, quiet-day diurnal variations, and worldwide storms), $\vec{j^Q}$ can be represented as a linear transformation of some independent vector $\vec{A}$ (either real or complex) realized using a linear operator $\hat{a}$:

$$\vec{j^Q}(\vec{r}) = \hat{a}(\vec{r})\vec{A}/T, \tag{2.5}$$

The vector $\vec{A}$ is independent of the coordinate system. It characterizes the polarization and strength of the currents flowing in the ionosphere and magnetosphere, and is called the *vector field characteristic*.

The operator $\hat{a}$ in a general case depends on the spatial coordinates and characterizes the geometry of the external currents, that is, the excitation of the magneto-telluric field. It is called the *excitation operator*. The excitation operator does not change for one specific type of variations (micropulsations, microstorms, $S_q$variations, worldwide storms), but may change from one type of variation to another.

Equation (2.5) is substituted into (2.4). Then

$$\vec{E}(\vec{r},\omega) = \hat{e}(\vec{r},\omega,\sigma)\vec{A},$$

$$\vec{H}(\vec{r},\omega) = \hat{h}(\vec{r},\omega,\sigma)\vec{A}, \tag{2.6}$$

where

$$\hat{e}(\vec{r},\omega,\sigma) = \iiint_Q \hat{G}^E\left(\vec{r}\middle|\vec{r'},\omega,\sigma\right)\hat{a}\left(\vec{r'}\right)dv',$$

$$\hat{h}(\vec{r},\omega,\sigma) = \iiint_Q \hat{G}^H\left(\vec{r}\middle|\vec{r'},\omega,\sigma\right)\hat{a}\left(\vec{r'}\right)dv'. \tag{2.7}$$

One can see that the operators $\hat{e}$ and $\hat{h}$ depend on the coordinates of the observation point, $\vec{r}$, the frequency, ω, and the distribution of electrical conductivity in the medium, σ. These are called the electrical and magnetic characteristic field operators. It must be stressed that, while these operators, as well as the excitation operator, $\hat{a}$, are constant with respect to a given type of excitation, they can change as one type of variation is replaced by another (as, for example, the transition from observations of storm-time variations to quiet-time variations).

If it is assumed that both characteristic operators, $\hat{e}$ and $\hat{h}$, are invertible (that is, inverse operators $\hat{e}^{-1}$ and $\hat{h}^{-1}$ exist), then, in accord with equations (2.6) and (2.7),

$$\vec{A} = \begin{Bmatrix} \hat{e}^{-1}(\vec{r},\omega,\sigma)\vec{E}(\vec{r},\omega) \\ \hat{h}^{-1}(\vec{r},\omega,\sigma)\vec{H}(\vec{r},\omega) \end{Bmatrix}. \tag{2.8}$$

Substituting the bottom expression from equation (2.8) into (2.6) and the top expression from equation (2.8) into (2.7), the following is obtained:

$$\vec{E}(\vec{r},\omega) = \hat{e}(\vec{r},\omega,\sigma)\hat{h}^{-1}(\vec{r},\omega,\sigma)\vec{H}(\vec{r},\omega) = \hat{Z}(\vec{r},\omega,\sigma)\vec{H}(\vec{r},\omega),$$

$$\vec{H}(\vec{r},\omega) = \hat{h}(\vec{r},\omega,\sigma)\hat{e}^{-1}(\vec{r},\omega,\sigma)\vec{E}(\vec{r},\omega) = \hat{Y}(\vec{r},\omega,\sigma)\vec{E}(\vec{r},\omega). \tag{2.9}$$

Here, $\hat{Z}$ and $\hat{Y}$ are operators representing impedance and admittance, respectively:

$$\hat{Z}(\vec{r},\omega,\sigma) = \hat{e}(\vec{r},\omega,\sigma)\hat{h}^{-1}(\vec{r},\omega,\sigma),$$

$$\hat{Y}(\vec{r},\omega,\sigma) = \hat{h}(\vec{r},\omega,\sigma)\hat{e}^{-1}(\vec{r},\omega,\sigma). \tag{2.10}$$

If $\vec{E}$ and $\vec{H}$ are measured at several points on the earth's surface (with radius vectors $\vec{r}$ and $\vec{r_0}$), then, using equations (2.6), (2.7), and (2.8), one can write

$$\vec{E}(\vec{r},\omega) = \hat{e}(\vec{r},\omega,\sigma)\hat{e}^{-1}(\vec{r_0},\omega,\sigma)\vec{E}(\vec{r_0},\omega) = \hat{t}(\vec{r}|\vec{r_0},\omega,\sigma)\vec{E}(\vec{r_0}),$$

$$\vec{H}(\vec{r},\omega) = \hat{h}(\vec{r},\omega,\sigma)\hat{h}^{-1}(\vec{r_0},\omega,\sigma)\vec{H}(\vec{r_0},\omega) = \hat{m}(\vec{r}|\vec{r_0},\omega,\sigma)\vec{H}(\vec{r_0}). \tag{2.11}$$

Here, $\hat{t}$ and $\hat{m}$ are telluric and magnetic operators:

$$\hat{t}(\vec{r}|\overrightarrow{r_0},\omega,\sigma) = \hat{e}(\vec{r},\omega,\sigma)\hat{e}^{-1}(\overrightarrow{r_0},\omega,\sigma),$$

$$\hat{m}(\vec{r}|\overrightarrow{r_0},\omega,\sigma) = \hat{h}(\vec{r},\omega,\sigma)\hat{h}^{-1}(\overrightarrow{r_0}\omega,\sigma). \quad (2.12)$$

The operators $\hat{Z}$, $\hat{Y}$, $\hat{t}$, and $\hat{m}$, are called the magnetotelluric operators. The four operators evoke the transformation of the electric and magnetic fields one to the other. Each type of magnetotelluric variation is characterized by its own set of operators, $\hat{Z}$, $\hat{Y}$, $\hat{t}$, and $\hat{m}$, which depends only on frequency, the location of the observation point, the strength and orientation of the ionospheric and magnetospheric currents, and the distribution of electrical conductivity in the medium, σ.

The magnetotelluric operators on a given set of basic functions have corresponding matrices, which are called the *magnetotelluric matrices*. Differences in these matrices reflect differences in the types of variations being observed. For micropulsations and storm-time excitation observed at low to mid-latitudes (that is, for the variations which are most commonly used in geophysical exploration because of the frequency window), the dimensionality of the magnetotelluric matrix is twofold (Berdichevskiĭ and Zhdanov, 1984). For such fields, if the horizontal components of the electric and magnetic fields are recorded, the matrix operators $\hat{Z}$, $\hat{Y}$, $\hat{t}$, and $\hat{m}$, in accord with the rules of linear algebra, take the following forms:

$$[Z_{\alpha\beta}] = \begin{bmatrix} Z_{xx} & Z_{xy} \\ Z_{yx} & Z_{yy} \end{bmatrix}, \quad (2.13)$$

$$[Y_{\alpha\beta}] = \begin{bmatrix} Y_{xx} & Y_{xy} \\ Y_{yx} & Y_{yy} \end{bmatrix}, \quad (2.14)$$

$$[t_{\alpha\beta}] = \begin{bmatrix} t_{xx} & t_{xy} \\ t_{yx} & t_{yy} \end{bmatrix}, \quad (2.15)$$

$$[m_{\alpha\beta}] = \begin{bmatrix} m_{xx} & m_{xy} \\ m_{yx} & m_{yy} \end{bmatrix}. \quad (2.16)$$

Consequently, in cases of operator relationships, equations (2.13), (2.14), (2.15), and (2.16), one can write (Berdichevskiĭ and Zhdanov, 1984)

$$E_x = Z_{xx}H_x + Z_{xy}H_y,$$

$$E_y = Z_{yx}H_x + Z_{yy}H_y, \tag{2.17}$$

$$H_x = Y_{xx}E_x + Y_{xy}E_y,$$

$$H_y = Y_{yx}E_x + Y_{yy}E_y, \tag{2.18}$$

$$E_x = t_{xx}E_x(\overrightarrow{r_0}) + t_{xy}E_y(\overrightarrow{r_0}),$$

$$E_y = t_{yx}E_x(\overrightarrow{r_0}) + t_{yy}E_y(\overrightarrow{r_0}), \tag{2.19}$$

$$H_x = m_{xx}H_x(\overrightarrow{r_0}) + m_{xy}H_y(\overrightarrow{r_0}),$$

$$H_y = m_{yx}H_x(\overrightarrow{r_0}) + m_{yy}H_y(\overrightarrow{r_0}). \tag{2.20}$$

2.2 Induction vectors and tippers

Besides the MT method, modern magnetotellurics consists of another branch, the magnetovariational (MV) method, which studies the linear transformation of the magnetic field.

Zhdanov (2009) has demonstrated that, when surveys are carried out in regions with a horizontally inhomogeneous geoelectric structure, the magnetic field $\vec{H}$ will have a significant vertical component (of course, the earth's steady magnetic field has a significant vertical component, H_z, almost everywhere, but it does not contribute to electromagnetic induction). In the case of a sea-bottom magnetoteluric survey over an area with a horizontally inhomogeneous geoelectric structure, the electric field $\vec{E}$ will have a significant vertical component E_z. In the theory of linear relationships, it can be shown that,

in cases of linear correlations of the type given in equations (2.17) through (2.20), supplementary formulas can be used (Zhdanov, 2009):

$$H_z = W_{zx}H_x + W_{zy}H_y, \tag{2.21}$$

$$E_z = V_{zx}E_x + V_{zy}E_y. \tag{2.22}$$

Relationship (2.21) bears the name Wiese-Parkinson relationship. Formula (2.22) is an electric analog of the Wiese-Parkinson relationship (Parkinson, 1959, 1962). These relationships reflect the fact that the vertical components of the magnetic field H_z or the electric field E_z at every point are linearly related to the horizontal components of the same field. As was the case with the various linear relationships described earlier, the coefficients of the Wiese-Parkinson relationship and its electric analog depend only on the coordinates of the observation point, $\vec{r}$, the frequency, ω, and the distribution of electrical conductivity in the medium. The values W_{zx} and W_{zy}, V_{zx}, and V_{zy} form complex vectors:

$$\overrightarrow{W} = W_{zx}\overrightarrow{d_x} + W_{zy}\overrightarrow{d_y}, \tag{2.23}$$

$$\vec{V} = V_{zx}\overrightarrow{d_x} + V_{zy}\overrightarrow{d_y}. \tag{2.24}$$

in which the real and imaginary parts are as follows:

$$\mathrm{Re}\left(\overrightarrow{W}\right) = \mathrm{Re}W_{zx}\overrightarrow{d_x} + \mathrm{Re}W_{zy}\overrightarrow{d_y}, \mathrm{Im}\left(\overrightarrow{W}\right) = \mathrm{Im}W_{zx}\overrightarrow{d_x} + \mathrm{Im}W_{zy}\overrightarrow{d_y}, \tag{2.25}$$

$$\mathrm{Re}\left(\vec{V}\right) = \mathrm{Re}V_{zx}\overrightarrow{d_x} + \mathrm{Re}V_{zy}\overrightarrow{d_y}, \mathrm{Im}\left(\vec{V}\right) = \mathrm{Im}V_{zx}\overrightarrow{d_x} + \mathrm{Im}V_{zy}\overrightarrow{d_y}. \tag{2.26}$$

Vector $\overrightarrow{W}$ is named the Wiese-Parkinson vector, or the induction vector. Vector $\overrightarrow{W}$ is often called a (magnetic) *tipper*.

By analogy, we will call vector $\vec{V}$ an *electric tipper*. Note that on land, the vertical component of an electric field is negligibly small, $E_z = 0$, which results in a linear relationship between the horizontal components of the electric field:

$$V_{zx}\overrightarrow{E_x} + V_{zy}\overrightarrow{E_y} = 0. \quad (2.27)$$

However, in the case of measurements conducted on the sea bottom, $E_z = 0$, and the electric tipper reflects the horizontal inhomogeneities of the sea-bottom formations.

In summary, it has been shown that for an arbitrary distribution of electrical conductivity in the earth, a linear functional relationship of the type in equations (2.17) through (2.22) exists between the components of the magnetotelluric field. The coefficients in these linear relationships (that is, the elements of the magnetotelluric matrix) are *transfer functions*. The elements of the magnetotelluric matrix are invariant on rotation: they reflect the distribution of electrical conductivity in the earth, but are independent of changes in the sources of the field, the magnetospheric and ionospheric currents. The transfer functions are also called *electrical conductivity functions*. The electrical conductivity functions, in contrast to measured electric and magnetic fields, carry information about the internal geoelectric structure of the earth only. Determining the electrical conductivity function is the basic step in application of the magnetotelluric method.

Determination of the conductivity function can be accomplished through the use of statistical analysis methods including cross- and auto-correlation of field components and calculation of the coefficients of multiple linear regressions. The techniques currently in use for determining the magnetotelluric matrix will be reviewed in detail in the following sections.

It is noted in conclusion that the linear operators can be considered as examples of rather more esoteric objects in linear algebra: tensors. Frequently, magnetotelluric operators are called magnetotelluric tensors, and we speak of *tensor impedance*, *tensor admittance*, and *telluric* and *magnetic tensors*. In this thesis, in order to retain some

simplicity in mathematical presentation, we will accept the linear operator approach and only mention the use of the tensor terminology (Zhdanov, 2009).

2.3 Principles of the ZTEM method

The z-axis tipper electromagnetic (ZTEM) system measures the transfer functions (tippers) of audio-frequency natural sources using an airborne receiver at the vertical magnetic field and a pair of orthogonal horizontal magnetic field receivers at a base station. Data are typically measured from 30 Hz to 720 Hz, giving detection depths down to 1 km or more, depending on the conductivity of the terrain. The airborne deployment makes it possible to acquire ZTEM data over large areas for a relatively low cost compared to equivalent ground surveys. This makes it a practical method for mapping large-scale geological structures. As an airborne extension of the magnetovariational (MV) method, the ZTEM transfer functions contain information about the 3D conductivity distribution within the earth. A rigorous 3D inversion algorithm for regularized inversion of ZTEM data based on the integral equation method (Zhdanov et al., 2011) is presented in this section.

In the air, ZTEM instrumentation uses a helicopter to tow a coil developed by Geotech Inc., which measures the vertical component of the magnetic field. The horizontal magnetometers located in the reference station measure horizontal components of the magnetic field. The essential components of the system are shown in Figure 1.

As mentioned above, the ZTEM system measures the transfer functions that relate the vertical magnetic fields observed above the earth to the horizontal magnetic field at some fixed reference station. This relation is given by the following formula:

$$H_z(\vec{r}) = T_{zx}(\vec{r}, \overrightarrow{r_0})H_x(\overrightarrow{r_0}) + T_{zy}(\vec{r}, \overrightarrow{r_0})H_y(\overrightarrow{r_0}), \quad (2.28)$$

where $\vec{r}$ is the location of the airborne station, $\overrightarrow{r_0}$ is the location of the ground-based reference station, and T_{zx} and T_{zy} are the vertical field transfer functions. In order to determine two unknown transfer functions, the vertical fields are measured for two independent polarizations of the magnetic field. The fields for each polarization are given by the following expressions:

$$\begin{cases} H_z^1 = T_{zx}H_x^1 + T_{zy}H_y^1 \\ H_z^2 = T_{zx}H_x^2 + T_{zy}H_y^2 \end{cases}, \quad (2.29)$$

or in matrix form:

$$\begin{pmatrix} H_z^1(\vec{r}) \\ H_z^2(\vec{r}) \end{pmatrix} = \begin{pmatrix} H_x^1(\overrightarrow{r_0}) & H_y^1(\overrightarrow{r_0}) \\ H_x^2(\overrightarrow{r_0}) & H_y^2(\overrightarrow{r_0}) \end{pmatrix} \begin{pmatrix} T_{zx} \\ T_{zy} \end{pmatrix}, \quad (2.30)$$

where the superscript in equations (2.28) and (2.29) refer to the source field polarizations in the x and y directions, respectively. Solving equation (2.30), one finds the following expressions for the transfer functions:

$$\begin{cases} T_{zx} = \frac{H_y^2 H_z^1 - H_y^1 H_z^2}{H_x^1 H_y^2 - H_x^2 H_y^1} \\ T_{zy} = \frac{-H_x^2 H_z^1 + H_x^1 H_z^2}{H_x^1 H_y^2 - H_x^2 H_y^1} \end{cases}. \quad (2.31)$$

2.4 Principles of the AirMt method

The AirMt method has been developed by Geotech LTD. Figure 1 and Figure 2 show the coil which is used in AirMt method. It is based on measuring all three orthogonal components (Hx, Hy, and Hz) by airborne platform. However, it is difficult to keep the system frame fixed in the moving airborne platform. This difficulty is overcome by calculating the transfer functions as the ratio of the magnetic field components in the

airborne station and the horizontal magnetic field components in the reference ground station (Legault et al., 2012). The standard frequencies are between 30 and 720 Hz. The AirMt transfer functions can be calculated using the same principles as the conventional magnetovariational (MV) transforms (Berdichevskiĭ and Zhdanov, 1984).

Following Berdichevskii and Zhdanov (1984), the 3D magnetic field variations at an airborne platform can be related to the components of the horizontal magnetic fields measured at a base station by a three-row by two-column tensor $\hat{T}$ (Kuzmin et al., 2010):

$$\vec{H} = \hat{T}\vec{H^0}, \tag{2.32}$$

where $\vec{H}$ is the vector of the magnetic field measured at the receiver location, and $\vec{H^0}$ is the vector of the magnetic field measured at the reference station. Expression (2.32) can be written in matrix notation as follow:

$$\begin{bmatrix} H_x \\ H_y \\ H_z \end{bmatrix} = \begin{bmatrix} T_{xx} & T_{xy} \\ T_{yx} & T_{yy} \\ T_{zx} & T_{zy} \end{bmatrix} \begin{bmatrix} H_x^0 \\ H_y^0 \end{bmatrix}. \tag{2.33}$$

Similar to the tipper components (2.28), it is possible to express AirMT tensor components using two modes of the incident field: TM and TE. This expression uses the assumption that the reference field is measured far away from the anomalous region. The conductivity distribution below the reference station does not change in the inversion process and thus can be approximated by 1D distribution. It is known that in a 1D case, the TM mode H_x^0 component is zero, as is the TE mode H_y^0 component. This results in the following expressions for the receiver field components:

$$H_x^1 = T_{xx}H_x^0 + T_{xy}H_y^0 = T_{xy}H_y^0$$

$$H_x^2 = T_{xx}H_x^0 + T_{xy}H_y^0 = T_{xx}H_x^0$$

$$H_y^1 = T_{yx}H_x^0 + T_{yy}H_y^0 = T_{yy}H_y^0$$

$$H_y^2 = T_{yx}H_x^0 + T_{yy}H_y^0 = T_{yx}H_x^0$$

$$H_z^1 = T_{zx}H_x^0 + T_{zy}H_y^0 = T_{zy}H_y^0$$

$$H_z^2 = T_{zx}H_x^0 + T_{zy}H_y^0 = T_{zx}H_x^0, \qquad (2.34)$$

where superscript 1 indicates the TM mode, and superscript 2 stands for the TE mode. Note that, in a case of the conductivity distributions close to the 1D reference station's distribution, the AirMt tensor components take the following values:

$$T_{xy} \approx T_{yx} \approx T_{zx} \approx 0$$

$$T_{xx} \approx T_{yy} \approx T_{zz} \approx 1. \qquad (2.35)$$

Based on (2.34), the AirMt tensor takes the following form:

$$\hat{T} = \left[\overrightarrow{T_1} \quad \overrightarrow{T_2}\right] = \begin{bmatrix} \frac{H_x^2}{H_x^0} & \frac{H_x^1}{H_y^0} \\ \frac{H_y^2}{H_x^0} & \frac{H_y^1}{H_y^0} \\ \frac{H_z^2}{H_x^0} & \frac{H_z^1}{H_y^0} \end{bmatrix}. \qquad (2.36)$$

The cross product of the AirMt vectors $\overrightarrow{T_1}$ and $\overrightarrow{T_2}$ can be written as follows:

$$\vec{K} = \overrightarrow{T_1} \times \overrightarrow{T_2} = \frac{1}{H_x^0 H_y^0}\left[H_y^2H_z^1 - H_y^1H_z^2 \quad H_x^1H_z^2 - H_x^2H_z^1 \quad H_x^2H_y^1 - H_x^1H_y^2\right]. \qquad (2.37)$$

Finally, compact amplification parameter $\vec{P}$ is expressed as the function of $\vec{K}$:

$$\vec{P} = \vec{K} \cdot \mathrm{Re}(\vec{K}) / \left|\mathrm{Re}(\vec{K})\right| = \frac{K_1\mathrm{Re}(K_1)+K_2\mathrm{Re}(K_2)+K_3\mathrm{Re}(K_3)}{\sqrt{\mathrm{Re}(K_1)^2+\mathrm{Re}(K_2)^2+\mathrm{Re}(K_3)^2}} \qquad (2.38)$$

It can be shown (Kuzmin et al., 2010) that $\vec{P}$ is invariant under any rotation of the airborne frame of reference or the base station frame of reference. This fact gives AirMt an advantage from both measurement and interpretation standpoints. During the measurements, an operator does not need to keep the aircraft and airborne receiver aligned

with the reference system. An interpretation specialist can use a coordinate system independent of the measurement.

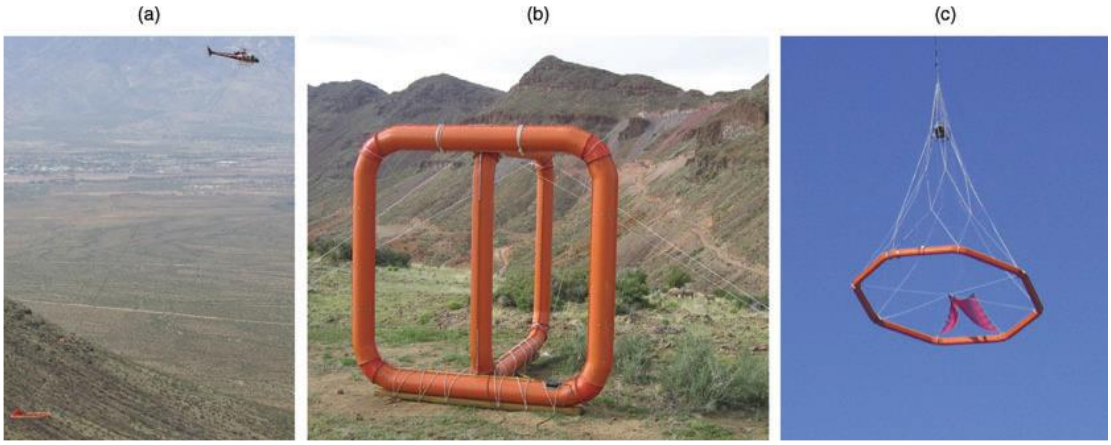

Figure 1. Coil used in the ZTEM method, (a) Helicopter flying a coil to measure the vertical magnetic field. (b) Ground-based reference station. (c) Coil used to measure the vertical fields (adopted from TechnoImaging, 2011)

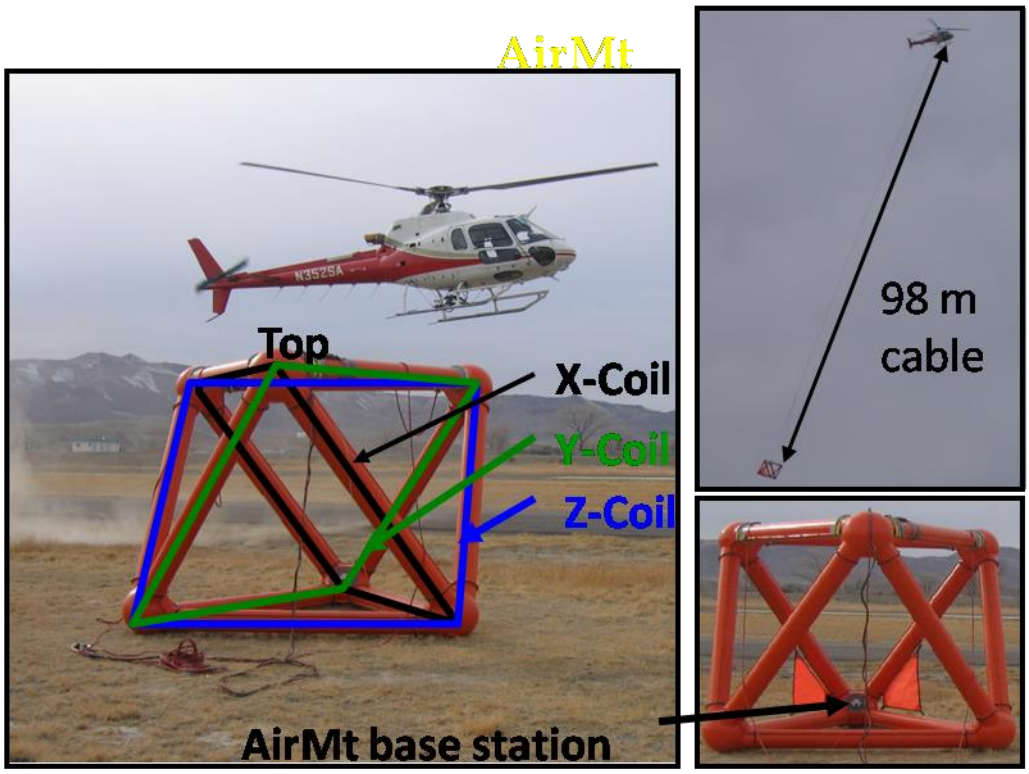

Figure 2. The coils used in air and ground-base station, adopted from TechnoImaging.

CHAPTER 3

FORWARD MODELING OF ZTEM AND AIRMT DATA

In the final decade of the twentieth century and in the beginning of the twenty-first century, methods for numerical and analytical modeling of the interaction of electromagnetic fields with the earth structures were developed rapidly. This development was driven by the availability of high-performance computers, including PC clusters, with which such models could be constructed. This modeling capability made possible the extraction of much more information from the field data than had been possible previously when only heuristic interpretation was feasible. The modern capability of geoelectrical methods is based on two technological developments: the ability to acquire great volumes of data with high accuracy, and the possibility of extracting sophisticated models of geoelectrical structures from these data using advanced numerical modeling and inversion methods (Zhdanov, 2009).

There are several techniques available for electromagnetic forward modeling. The finite-difference and integral equation methods are the most widely used. Other methodologies include the finite-element and finite-volume methods. The integral equation method is a powerful tool in three-dimensional (3D) electromagnetic modeling for geophysical applications. It was introduced originally in the pioneering paper by Dmitriev

(1969), which was published in Russian and long remained unknown to Western geophysicists (as well as the work of Tabarovsky, 1975). More than 40 years ago, practically simultaneously, Raiche (1974), Weidelt (1975), and Hohmann (1975) published their famous papers on the IE method. Many more researchers have contributed to the improvement and development of this method in recent years (Abubakar and van den Berg, 2004; Avdeev, 2005; Dmitriev and Nesmeyanova, 1992; Singer and Fainberg, 1997; Wannamaker, 1991; Xiong, 1992; Xiong and Kirsch, 1992; Zhdanov, 2002). The main advantage of the IE method in comparison with the FD and FE methods is the fast and accurate simulation of the EM response in models with relatively local 3D anomalies in a layered background.

In this chapter, the principles of the IE method and how to forward model ZTEM and AirMt data by using the IE method will be introduced.

3.1 Principles of EM forward modeling using the integral equation method

This section considers a 3D geoelectrical model with a normal (background) complex conductivity σ_b and local inhomogeneity D with an arbitrarily varying complex conductivity $\sigma = \sigma_b + \Delta\sigma$. Our study will be confined to consideration of nonmagnetic media and, hence, it will be assumed that $\mu = \mu_0 = 4\pi \times 10^{-7}\ \mathrm{H/m}$, where μ_0 is the free-space magnetic permeability. The model is excited by an electromagnetic field generated by an arbitrary source with an extraneous current distribution $\vec{j^Q}$ concentrated within some local domain Q. This field is time harmonic as $e^{-i\omega t}$. In order to derive the integral equations for the electromagnetic field for this model, the normal (background) and anomalous electromagnetic fields must be introduced.

The electromagnetic field in the model described above can be presented as a sum of the background (normal) and anomalous fields:

$$\vec{E} = \overrightarrow{E^b} + \overrightarrow{E^a}, \vec{H} = \overrightarrow{H^b} + \overrightarrow{H^a}, \tag{3.1}$$

where the background field is a field generated by the given sources in the model with the background (normal) distribution of conductivity σ_b, and the anomalous field is produced by the anomalous conductivity distribution $\Delta\sigma$.

The total electromagnetic field in this model satisfies Maxwell's equations:

$$\nabla \times \vec{H} = \sigma\vec{E} + \overrightarrow{j^Q}$$

$$\nabla \times \vec{E} = i\omega\mu_0\vec{H}, \tag{3.2}$$

which can be written separately for the background field $\overrightarrow{E^b}$, $\overrightarrow{H^b}$,

$$\nabla \times \overrightarrow{H^b}, = \sigma\overrightarrow{E^b} + \overrightarrow{j^Q}$$

$$\nabla \times \overrightarrow{E^b} = i\omega\mu_0\overrightarrow{H^b}, \tag{3.3}$$

and for the anomalous field $\overrightarrow{E^a}$, $\overrightarrow{H^a}$,

$$\nabla \times \overrightarrow{H^a}, = \sigma\overrightarrow{E^a} + \overrightarrow{j^Q}$$

$$\nabla \times \overrightarrow{E^a} = i\omega\mu_0\overrightarrow{H^a}, \tag{3.4}$$

where $\overrightarrow{j^Q}$ is the density of extraneous electric currents, and

$$\overrightarrow{j^a}(\vec{r}) = \Delta\sigma(\vec{r})\vec{E}(\vec{r}) = \Delta\sigma(\vec{r})\left[\overrightarrow{E^b}(\vec{r}) + \overrightarrow{E^a}(\vec{r})\right], \tag{3.5}$$

is the density of excess (anomalous) electric currents within the inhomogeneity D. Equations (3.4) follow from the previous equations by subtraction.

According to the integral form of Maxwell's equations (Zhdanov, 2002), the anomalous field in the frequency domain can be represented as an integral over the excess anomalous currents, $\overrightarrow{j^a} = \Delta\sigma\vec{E}$, in the inhomogeneous domain, D:

$$\overrightarrow{E^a}(\vec{r}_j) = \widehat{G_E}(\Delta\sigma\vec{E}) = \iiint_D \widehat{G_E}(\vec{r}_j|\vec{r})\,\Delta\sigma(\vec{r})\vec{E}(\vec{r})dv, \tag{3.6}$$

$$\overrightarrow{H^a}(\vec{r}_j) = \widehat{G_H}(\Delta\sigma\vec{E}) = \iiint_D \widehat{G_H}(\vec{r}_j|\vec{r})\,\Delta\sigma(\vec{r})\vec{E}(\vec{r})dv. \tag{3.7}$$

If equations (3.6) and (3.7) are substituted to equation (3.1), then

$$\vec{E}(\vec{r}_j) = \overrightarrow{E^b}(\vec{r}_j) + \iiint_D \widehat{G_E}(\vec{r}_j|\vec{r})\,\Delta\sigma(\vec{r})\vec{E}(\vec{r})dv, \tag{3.8}$$

$$\vec{H}(\vec{r}_j) = \overrightarrow{H^b}(\vec{r}_j) + \iiint_D \widehat{G_H}(\vec{r}_j|\vec{r})\,\Delta\sigma(\vec{r})\vec{E}(\vec{r})dv, \tag{3.9}$$

where $\widehat{G_{E,H}}(\vec{r}_j|\vec{r})$ stands for the electric or magnetic Green's tensors defined for an unbounded conductive medium with background conductivity σ_b .

3.2 Forward modeling of ZTEM data

ZTEM data are very similar to magnetovariational (MV) data. This section begins with a discussion of ZTEM transfer functions by reviewing the MV principles. When surveys are carried out in regions with a horizontally inhomogeneous geoelectric structure, the magnetic field, generated by a vertically propagated plane external field, will have a significant vertical component. Based on linear relationships between the different magnetic field components, the following relationship can be shown (Berdichevskii and Zhdanov, 1984):

$$H_z = W_{zx}H_x + W_{zy}H_y. \tag{3.10}$$

This relationship is called the Weiss-Parkinson relationship. It reflects the fact that the vertical component of the magnetic field H_z at every point is linearly related to the horizontal components of the same field. It was demonstrated by Berdichevskii and Zhdanov (1984) that the coefficients of the Weiss-Parkinson relationship depend on the coordinates of the observation point, the frequency, and the distribution of electrical

conductivity in the medium only. The values W_{zx} and W_{zy} form a complex vector, named the Weiss-Parkinson vector, or induction vector, or the tipper. In what follows, the term tipper is used. The tipper, in contrast to the measured magnetic field, contains information about the internal geoelectrical structure of the earth independent of the magnetic field's source. The tipper components can be determined from the following system of equations:

$$H_z^1 = W_{zx}H_x^1 + W_{zy}H_y^1$$

$$H_z^2 = W_{zx}H_x^2 + W_{zy}H_y^2, \tag{3.11}$$

where upper indices 1 and 2 correspond to different polarizations of the plane wave external field.

The solution to this system is expressed as follows:

$$W_{zx} = \frac{H_y^2 H_z^1 - H_y^1 H_z^2}{H_x^1 H_y^2 - H_x^2 H_y^1}, W_{zy} = \frac{H_x^1 H_z^2 - H_x^2 H_z^1}{H_x^1 H_y^2 - H_x^2 H_y^1}. \tag{3.12}$$

The geophysical technique based on measuring the tipper and subsequently determining the conductivity distribution constitutes the magnetovariational (MV) method.

The vertical component of the magnetic field, H_z, can be measured from the air. Airborne surveys can cover large areas and collect data in an efficient manner. To be able to apply the MV method, one needs to know the values of the horizontal magnetic field components, H_x and H_y, at the same locations as the vertical component, H_z. Unfortunately, accurate airborne measurement of the horizontal components is technically challenging. However, it was shown by Berdichevskii and Zhdanov (1984) that magnetovariational transfer functions, similar to a conventional tipper, can be calculated using the measurements of the horizontal field components, H_{x0} and H_{y0}, at a fixed reference station only. Then

$$H_z = W_{zx}^{ZTEM} H_{x0} + W_{zy}^{ZTEM} H_{y0}. \quad (3.13)$$

Provided two measurements of the fields in two different polarizations, ZTEM tippers take the following form:

$$W_{zx} = \frac{H_{y0}^2 H_z^1 - H_{y0}^1 H_z^2}{H_{x0}^1 H_{y0}^2 - H_{x0}^2 H_{y0}^1}, W_{zy} = \frac{H_{x0}^1 H_z^2 - H_{x0}^2 H_z^1}{H_{x0}^1 H_{y0}^2 - H_{x0}^2 H_{y0}^1}. \quad (3.14)$$

In modeling ZTEM data, we use equation (3.7), which connects the observed magnetic field at the receivers with the electric field inside the anomalous domain, D, representing a *field equation.* Writing equation (3.6) for the points within the anomalous domain, $\vec{r_j} \in D$, we arrive at a domain equation. In the integral equation formulation, the difficulty is finding the anomalous electric fields inside the domain since the equation is nonlinear. Once these have been found, it is straightforward to find the anomalous or total magnetic fields measured at the receivers using equations (3.7) or (3.1)

The ZTEM forward modeling problem can be described by the following operator equation:

$$d = A(m) = A(\Delta\sigma), \quad (3.15)$$

where d stands for the data vector formed by the components of the ZTEM tipper, A is the nonlinear forward operator encapsulating the governing equations of the ZTEM forward modeling problem described above, and m is the distribution of variations of the conductivity. To find specific components of an EM field, we solve the 3D forward modeling problem, using the contraction integral equation method (Hursán and Zhdanov, 2002; Zhdanov, 2009). These components are substituted in equations (3.14) for the tipper.

3.3 Forward modeling of AirMt data

In a general case, the 3D magnetic field variations at an airborne receiver platform to the horizontal fields measured at a base station are related by a three-row by two-column tensor $\widehat{T}$ (Berdichevskiĭ and Zhdanov, 1984):

$$\vec{H} = \widehat{T}\overrightarrow{H^0}\,, \tag{3.16}$$

which can be expressed in a matrix notation as follows:

$$\begin{bmatrix} H_x \\ H_y \\ H_z \end{bmatrix} = \begin{bmatrix} T_{xx} & T_{xy} \\ T_{yx} & T_{yy} \\ T_{zx} & T_{zy} \end{bmatrix} \begin{bmatrix} H_x^0 \\ H_y^0 \end{bmatrix}. \tag{3.17}$$

This results in the expressions (2.34), (2.35), and (2.36). According to the formula (2.37), finally, compact amplification parameter $\vec{P}$ is expressed as the function of $\vec{K}$:

$$\vec{P} = \vec{K} \cdot \mathrm{Re}(\vec{K}) / \left|\mathrm{Re}(\vec{K})\right| = \frac{K_1 \mathrm{Re}(K_1) + K_2 \mathrm{Re}(K_2) + K_3 \mathrm{Re}(K_3)}{\sqrt{\mathrm{Re}(K_1)^2 + \mathrm{Re}(K_2)^2 + \mathrm{Re}(K_3)^2}}. \tag{3.18}$$

where $\vec{K}$ is determined by formula (2.37), substituting expression (3.6) and (3.7) into formula (3.23), we calculate the compact amplification parameter, $\vec{P}$, using IE method.

CHAPTER 4

INVERSION OF ZTEM AND AIRMT DATA

Electromagnetic (Berdichevskiĭ and Zhdanov) inverse methods are widely used in the interpretation of geophysical EM data in mineral, hydrocarbon, and groundwater exploration. During the last decade, we have observed remarkable progress in the development of a multidimensional interpretation technique. Many papers have been published during the last 20 years on 3D inversion of EM geophysical data (Alumbaugh and Newman, 1997; Gribenko and Zhdanov, 2007; Mackie and Watts, 2004; Madden and Mackie, 1989; Newman and Alumbaugh, 1997; Siripunvaraporn et al., 2005; Zhdanov and Fang, 1996; Zhdanov et al., 2000; Zhdanov and Golubev, 2003; Zhdanov and Tartaras, 2002). However, EM inversion is still one of the most difficult problems of EM geophysics.

Nowadays there are several algorithms available for rigorous 3D MT inversion, such as the Gauss-Newton method (Farquharson et al., 2002; Sasaki, 2004; Siripunvaraporn et al., 2005), the quasi-Newton method (Avdeev and Avdeeva, 2006), and the nonlinear conjugate gradient method (Gribenko et al., 2010; Newman and Alumbaugh, 2000; Zhdanov and Golubev, 2003). In this chapter, the reweighted regularized conjugate gradient (RRCG) method will be introduced to formulate the ZTEM and AirMt data inversion problem. The regularized conjugate gradient method based on the adaptive regularization and minimum-norm (MN) stabilizer is used to solve the minimization

problem of this parametric functional. The quasi-Born (QB) approximation and the receiver footprint approach for computing and storing Frechet derivatives will also be discussed in this chapter, and how to calculate the Frechet derivative for both ZTEM and AirMt data will be presented as well.

4.1 Principles of regularized geophysical inversion

The ZTEM and AirMt forward modeling problem can be described by the following operator equation:

$$\mathrm{d}^{\mathrm{ZTEM}} = \mathrm{A}^{\mathrm{ZTEM}}(\Delta\sigma), \;\; \mathrm{d}^{\mathrm{AirMt}} = \mathrm{A}^{\mathrm{AirMt}}(\Delta\sigma), \tag{4.1}$$

where d stands for the data vector formed by the components of the ZTEM tipper and/or AirMt amplification parameter, and A is the nonlinear forward operator encapsulating the governing equations of the ZTEM and AirMt forward modeling problem described in the previous sections.

The inverse problem described by equation (4.1) is ill posed, i.e., the solution is nonunique and unstable. As per the MT and MV methods, Tikhonov regularization is used to solve this problem which is based on minimization of the Tikhonov parametric functional:

$$\mathrm{P}(\Delta\sigma) = \|\mathrm{A}(\Delta\sigma) - \mathrm{d}\|_2^2 + \alpha\|\mathrm{W_m}(\Delta\sigma) - \mathrm{W_m}\Delta\sigma^{\mathrm{apr}}\|_2^2 = \min, \tag{4.2}$$

where $\mathrm{W_m}$ is some real weighting matrix of model parameters, $\Delta\sigma^{\mathrm{apr}}$ is some a priori anomalous conductivity distribution, $\|...\|$ denotes the Euclidean norm in the spaces of data and models, and α is the regularization parameter. The model weights are frequency dependent.

It was demonstrated in Zhdanov (2002) that the optimal choice of the model

parameter weighting matrix, W_m, is the square root of the integrated sensitivity matrix according to the following formula:

$$A = \sqrt{F^T F}, \tag{4.3}$$

$$W_m = \sqrt{\mathrm{diag}(A)}, \tag{4.4}$$

$$W_m = \sqrt[4]{\mathrm{diag}(F^T F)}. \tag{4.5}$$

where F is Frechet derivative.

Gradient-type methods are commonly used as an iterative way to solve the minimization problem of the parametric functional, such as the steepest descent method, the Newton method, the generalized minimum residual (GMRES) method, the minimum residual (MINRES) method, etc. In this thesis, the reweighted regularized conjugate gradient (RRCG) method is used to find the solution which minimizes the parametric functional with the minimum-norm stabilizer. The RRCG algorithm can be summarized as follows (Zhdanov, 2002):

$$r_n = A(m_n) - d$$

$$I_n^{\alpha_n} = I^{\alpha_n}(m_n) = F_{m_n}^T r_n + \alpha_n W_m^2 (m_n - m_{apr})$$

$$\beta_n^{\alpha_n} = \frac{\left\| I_n^{\alpha_n} \right\|^2}{\left\| I_{n-1}^{\alpha_{n-1}} \right\|^2}, \tilde{I}_n^{\alpha_n} = I_n^{\alpha_n} + \beta_n^{\alpha_n} \tilde{I}_{n-1}^{\alpha_{n-1}}$$

$$\tilde{k}_n^{\alpha_n} = \frac{\left(\tilde{I}_n^{\alpha_n T} \tilde{I}_n^{\alpha_n} \right)}{\left\{ \left\| F_{m_n} \tilde{I}_n^{\alpha_n} \right\|^2 + \alpha \left\| W_m \tilde{I}_n^{\alpha_n} \right\|^2 \right\}}$$

$$m_{n+1} = m_n - \tilde{k}_n^{\alpha_n} \tilde{I}_n^{\alpha_n}, \tag{4.6}$$

where $\tilde{k}_n^{\alpha_n}$ is the step length, $I_n^{\alpha_n}$ is the gradient direction computed using an adjoint operator.

In a practical inversion, $\tilde{k}_n^{\alpha_n}$ is computed using the following modified formula:

$$\tilde{k}_n^{\alpha_n} = k_c \cdot \frac{\left(\tilde{I}_n^{\alpha_n T} \tilde{I}_n^{\alpha_n}\right)}{\left\{\left\|F_{m_n} \tilde{I}_n^{\alpha_n}\right\|^2 + \alpha \left\|W_m \tilde{I}_n^{\alpha_n}\right\|^2\right\}}, \tag{4.7}$$

where k_c is the step length coefficient. It is a constant which can be set manually. This iterative process is terminated when the misfit reaches the given noise level ε_0:

$$\emptyset(m_N) = \|r_N\|^2 \leq \varepsilon_0 \, . \tag{4.8}$$

To apply the adaptive regularization method, the regularization parameter α is updated in the process of the iterative inversion as follows:

$$\alpha_n = \alpha_1 q^{n-1}, n = 1,2,3, \dots, 0 < q < 1. \tag{4.9}$$

4.2 Frechet derivative calculation and inversion of ZTEM data

As I demonstrated in Chapter 3, the *tippers* can be determined. The observed data in the ZTEM method consists of the components of the W_i vector, so in the ZTEM method, the Weiss-Parkinson relationship (3.12) is also used. It reflects the fact that the vertical component of the magnetic field H_z at every point is linearly related to the horizontal components of the same field:

$$H_z = W_{zx}^{ZTEM} H_{x0} + W_{zy}^{ZTEM} H_{y0}. \tag{4.10}$$

which can be found accords to the formulas:

$$W_{zx} = \frac{H_{y0}^2 H_z^1 - H_{y0}^1 H_z^2}{H_{x0}^1 H_{y0}^2 - H_{x0}^2 H_{y0}^1}, W_{zy} = \frac{H_{x0}^1 H_z^2 - H_{x0}^2 H_z^1}{H_{x0}^1 H_{y0}^2 - H_{x0}^2 H_{y0}^1}. \tag{4.11}$$

In order to use the RRCG method for the minimization of the parametric functional (4.2), it is necessary to calculate the derivative of the data parameters with respect to the model parameters, i.e., the Fréchet derivatives, otherwise known as the Jacobians or sensitivities. To calculate the Fréchet derivative of the ZTEM tippers with respect to the anomalous conductivity, $\Delta\sigma$, we apply a variational operator to equation (4.12). For the

W_{zx}^{ZTEM} component, the following is obtained:

$$\delta W_{zx}^{ZTEM} = \sum_{i=1,2}\left(\frac{\partial W_{zx}^{ZTEM}}{\partial H_z^i} F_{H_z^i}[\delta\Delta\sigma] + \sum_{\alpha=x0,y0}\frac{\partial W_{zx}^{ZTEM}}{\partial H_\alpha^i} F_{H_\alpha^i}[\delta\Delta\sigma]\right). \quad (4.12)$$

The expressions for the partial derivatives of the tippers with respect to the field components, necessary for the computation of equation (4.13), take the following forms:

$$\frac{\partial W_{zx}^{ZTEM}}{\partial H_{x0}^1} = -\frac{H_{y0}^2\left[H_{y0}^2 H_z^1 - H_{y0}^2 H_z^1\right]}{\left[H_{x0}^1 H_{y0}^2 - H_{x0}^2 H_{y0}^1\right]^2}, \quad (4.13)$$

$$\frac{\partial W_{zx}^{ZTEM}}{\partial H_{x0}^2} = \frac{H_{y0}^1\left[H_{y0}^2 H_z^1 - H_{y0}^1 H_z^2\right]}{\left[H_{x0}^1 H_{y0}^2 - H_{x0}^2 H_{y0}^1\right]^2}, \quad (4.14)$$

$$\frac{\partial W_{zx}^{ZTEM}}{\partial H_{y0}^1} = \frac{H_{y0}^2\left[H_{x0}^2 H_z^1 - H_{x0}^1 H_z^2\right]}{\left[H_{x0}^1 H_{y0}^2 - H_{x0}^2 H_{y0}^1\right]^2}, \quad (4.15)$$

$$\frac{\partial W_{zx}^{ZTEM}}{\partial H_{y0}^2} = \frac{H_{y0}^1\left[H_{x0}^1 H_z^1 - H_{x0}^2 H_z^1\right]}{\left[H_{x0}^1 H_{y0}^2 - H_{x0}^2 H_{y0}^1\right]^2}, \quad (4.16)$$

$$\frac{\partial W_{zx}^{ZTEM}}{\partial H_z^1} = \frac{H_{y0}^2}{H_{x0}^1 H_{y0}^2 - H_{x0}^2 H_{y0}^1}, \quad (4.17)$$

$$\frac{\partial W_{zx}^{ZTEM}}{\partial H_z^2} = \frac{-H_{y0}^1}{H_{x0}^1 H_{y0}^2 - H_{x0}^2 H_{y0}^1}. \quad (4.18)$$

Equation (4.12) contains the Fréchet derivatives F_H^i of the field components themselves, which are still unknown. Gribenko and Zhdanov (2007) described the quasi-analytical variable background (QAVB) method of Fréchet derivative computation:

$$F_{E,H}(r_j|r) = \left[\frac{1}{1-g^Q(r)}\widehat{G_{E,H}}(r_j|r) + \hat{K}(r_j|r)\right]E^n(r), \quad (4.19)$$

where:

$$g^Q(r) = \frac{E^Q(r)\cdot E^{b^*}(r)}{E^b(r)E^{b^*}(r)}. \quad (4.20)$$

E^Q is the quasi-Born approximation of the anomalous electric field:

$$E^Q = \widehat{G_E}[\Delta\sigma E^n], \quad (4.21)$$

and

$$\widehat{\mathrm{K}}(\mathrm{r_j}|\mathrm{r}) = \iiint_{\mathrm{D}} \frac{\Delta\sigma_\alpha(\mathrm{r}')}{\left(1-\mathrm{g^Q(r')}\right)^2} \widehat{\mathrm{G_E}}(\mathrm{r_j}|\mathrm{r}) \cdot \mathrm{E^b}(\mathrm{r}') \left[\frac{\mathrm{E^{b^*}}(\mathrm{r}')}{\mathrm{E^b}(\mathrm{r}')\cdot\mathrm{E^{b^*}}(\mathrm{r}')} \cdot \widehat{\mathrm{G_E}}(\mathrm{r}'|\mathrm{r})\right] \mathrm{dv}'. \quad (4.22)$$

Note that, in the case of a small conductivity perturbation, $\Delta\sigma_\alpha$, $\mathrm{g^Q(r)}$ tends to unity and $\widehat{\mathrm{K}}(\mathrm{r_j}|\mathrm{r})$ approaches zero. In this case, equation (4.19) reduces to the simplified form:

$$\mathrm{F_{E,H}}(\mathrm{r_j}|\mathrm{r}) = \widehat{\mathrm{G_{E,H}}}(\mathrm{r_j}|\mathrm{r})\mathrm{E^n}(\mathrm{r}). \quad (4.23)$$

For a number of test cases, application of quasi-Born (QB) equation (4.21) provides comparable accuracy to the QAVB Fréchet derivative. The advantage of the QB equation is that it does not require domain-to-domain electric Green's tensors $\widehat{\mathrm{G_E}}(\mathrm{r_j}|\mathrm{r})$, as are required in the QAVB equation (4.22). This results in reduced computational time, but most importantly in significant memory reduction. Note that the electric field $\mathrm{E^n}$ is computed from the IE forward modeling method. Therefore, no extra computation is required to compute the Fréchet derivative. To further reduce computational speed and computer memory requirements, we apply a moving footprint (Gribenko et al., 2010). The moving footprint assumes that, from a certain distance from a given receiver, the Fréchet derivative is sufficiently small that it can be neglected. This means that the Fréchet derivatives for cells beyond the footprint need not be stored.

4.3 Frechet derivative calculation and inversion of AirMt data

We have demonstrated in the previous chapters that, in a general case, the 3D magnetic field variations at an airborne receiver platform are related to the horizontal incident fields measured at a base station by a three-row by two-column tensor $\widehat{\mathrm{T}}$ like (4.24) (Berdichevskiĭ and Zhdanov, 1984):

$$\overrightarrow{\mathrm{H_R}} = \widehat{\mathrm{T}}\overrightarrow{\mathrm{H_B}}. \quad (4.24)$$

In a 2D case with Y as strike, then $\widehat{T_{YYB}} = 1$ (TM mode) and $\widehat{T_{XXB}}$ and $\widehat{T_{ZXB}}$ are the nonzero TE mode quantities. $\widehat{T_{XXB}}$ generally varies about 1, while $\widehat{T_{ZXB}}$ varies about 0. All other components are null in 2D. Note that the second field subscript refers to the base station.

We have also introduced function $\vec{K}$ which was immune to tilt errors:

$$\vec{K} = \left[-\widehat{T_{ZXB}}, 0, \widehat{T_{XXB}}\right]. \tag{4.25}$$

In the case of forward modeling, a simple approach is to assume that the base station observes the "primary" horizontal field directly, and the base station and airborne system are oriented in a fixed frame of reference. Then the first two columns of $\vec{T}$ are the vector magnetic fields in the airborne system (primary plus secondary) resulting from unit primary fields in the x and y directions, respectively, and the parameter $\vec{K}$ can be written as follows:

$$\vec{K} = \left[\overrightarrow{T_{yx}}\overrightarrow{T_{zy}} - \overrightarrow{T_{zx}}\overrightarrow{T_{yy}}, \overrightarrow{T_{zx}}\overrightarrow{T_{xy}} - \overrightarrow{T_{zz}}\overrightarrow{T_{zy}}, \overrightarrow{T_{xx}}\overrightarrow{T_{yy}} - \overrightarrow{T_{yx}}\overrightarrow{T_{xy}}\right]$$

$$\vec{K} = \vec{K} \cdot \mathrm{Re}(\vec{K}) / \left|\mathrm{Re}(\vec{K})\right|, \tag{4.26}$$

where $\overrightarrow{T_{yx}}$ is the y component of the complex magnetic field response at the airborne system to a unit primary field in the x direction.

The Frechet derivative of the AirMt response can be found as follows:

From the tipper element $\widehat{T_{ZXB}} = H_Z/H_{XB}$ and the horizontal element $\widehat{T_{XXB}} = H_X/H_{XB}$ in the 2D case, we have:

$$\partial\widehat{T_{ZXB}} = \partial H_Z/\partial H_{XB} - \partial H_{XB} H_Z/H_{XB}^2 = \left(\partial H_Z - \partial H_{XB}\widehat{T_{ZXB}}\right)/H_{XB}$$

$$\partial\widehat{T_{XXB}} = \partial H_X/\partial H_{XB} - \partial H_{XB} H_Z/H_{XB}^2 = \left(\partial H_X - \partial H_{XB}\widehat{T_{XXB}}\right)/H_{XB}, \tag{4.27}$$

where the ∂ derivative denotes the derivate with respect to $\partial\sigma_i$, and σ_i is the conductivity of the sub-region.

Similarly, $\partial\vec{K}$ must be derived from the derivative of the $\widehat{T_{ZXB}}$ and $\widehat{T_{XXB}}$ by application of the chain rule. This is a somewhat tedious but straightforward computation; we can find that the Fréchet derivative of the AirMt amplification parameter $\vec{P}$ in a 3D case is equal to the following expression:

$$\partial\vec{P} = \frac{1}{\sqrt{\sum_{i=1}^{3}\overrightarrow{K_i}\mathrm{Re}\left(\overrightarrow{K_i}\right)^2}} \times \left(\sum_{i=1}^{3}\partial\overrightarrow{K_i}\mathrm{Re}\left(\overrightarrow{K_i}\right) + \overrightarrow{K_i}\mathrm{Re}\left(\partial\overrightarrow{K_i}\right)\right)$$

$$-\frac{1}{\left(\sum_{i=1}^{3}\mathrm{Re}\left(\overrightarrow{K_i}\right)^2\right)^{3/2}} \times \sum_{i=1}^{3}\overrightarrow{K_i}\mathrm{Re}\left(\overrightarrow{K_i}\right) \cdot \sum_{i=1}^{3}\mathrm{Re}\left(\overrightarrow{K_i}\right)\mathrm{Re}\left(\partial\overrightarrow{K_i}\right), \qquad (4.28)$$

where $\overrightarrow{K_i}$ is equal to $\overrightarrow{K_1}, \overrightarrow{K_2}, \overrightarrow{K_3}$.

To find the derivatives of the components of the vector K, we apply a perturbation operator to the expressions (4.26):

$$\partial\overrightarrow{K_1} = \frac{1}{H_x^0 H_y^0}\left(\partial H_y^1 H_z^1 + H_y^2\,\partial H_z^1 - \partial H_y^1 H_z^2 - H_y^1\,\partial H_z^2\right)$$

$$\partial\overrightarrow{K_2} = \frac{1}{H_x^0 H_y^0}\left(\partial H_x^1 H_z^1 + H_x^1\,\partial H_z^2 - \partial H_x^1 H_z^1 - H_x^2\,\partial H_z^1\right)$$

$$\partial\overrightarrow{K_3} = \frac{1}{H_x^0 H_y^0}\left(\partial H_x^3 H_y^1 + H_x^2\,\partial H_y^1 - \partial H_x^1 H_y^2 - H_x^1\,\partial H_y^2\right). \qquad (4.29)$$

In deriving (4.29), we used the assumption that the reference station is located far from the anomalous region, making H_x^0 and H_y^0 constants.

Expressions (4.29) contain the Fréchet derivatives $F_{H_\alpha^i} = \partial H_\alpha^i$ of the field components themselves, which are still unknown. Gribenko and Zhdanov (2007) described the quasi-analytical variable background (QAVB) method of Fréchet derivative computation. A simplification of the QAVB, called quasi-Born, can be used:

$$F_{E,H}\left(r_j\middle|r\right) = \widehat{G_{E,H}}\left(r_j\middle|r\right)E^n(r). \qquad (4.20)$$

For the majority of test cases, application of the quasi-Born (QB) equation (4.30) provides the same accuracy as the QAVB Fréchet derivative. The advantage of the QB equation is that it does not require the domain-to-domain electric Green's tensors $\widehat{G_{E,H}}(r_j|r)$, which are required in the QAVB equation. This results in reduced computational time, but most importantly in significant memory reduction. Note that the electric field E^n is computed from the IE forward modeling method. Therefore, no extra computation is required to compute the Fréchet derivative. To further reduce computational speed and computer memory requirements, we apply a moving footprint approach (Cox et al., 2011). The moving footprint assumes that, from a certain distance from a given receiver, the Fréchet derivative is sufficiently small that it can be neglected. This means that the Fréchet derivatives for cells beyond the footprint need not be stored.

CHAPTER 5

MODEL STUDY OF THE INVERSION ALGORITHM

The ZTEM and AirMt transfer functions and the inversion algorithm have been discussed in the previous two chapters. In this chapter, the accuracy and stability of these two inversion algorithms will be tested for several different synthetic models and compared with the results based on two different sets of data. The basic test model is shown in Figure 3. The model consists of a 1 Ohm-m conductive L-shaped anomaly located inside a 100 Ohm-m host rock. Depth to the top of the anomaly is 600 m, and the thickness of the body is 400 m. The receivers are located in a 5×5 km^2 area, separated by 200 m for a total of 676 receiver positions with flight elevation 75 m above the surface. The reference receiver is placed on the surface about 7 km away from the modeling domain (X = 7500 m, Y = 7500 m). Synthetic data were computed at the standard set of ZTEM and AirMt frequencies: 30, 45, 90, 180, and 360 Hz. The parameters used in the basic model are listed in Table 1.

5.1 Inversion with true background conductivity

First, I have applied the inversion to the noise-free synthetic data using the true background conductivity, which was known.

The inversion domain was $6 \times 6 \times 3$ km^3, with inversion cell sizes $100 \times 100 \times 50$ m^3. The parameters used in the true model parameters inversion both in ZTEM and AirMt

data are shown in Table 2.

In the corresponding figures of inversion results, the white dashed line indicates the true model location of the L-shaped conductive target. Figure 4 shows the result of inversion of the synthetic ZTEM data. Both the location and conductivity of the L-shaped anomaly are recovered well. Figures 5 and 6 present maps of the observed and predicted ZTEM components, W_{zx} and W_{zy}. The result of inversion of the synthetic AirMt data is shown in Figure 7. AirMt inversion also recovered the L-shaped anomaly reasonably well. Maps of the observed and predicted AirMt amplification parameters are shown in Figure 8.

5.2 Inversion with inaccurate background conductivity

In real field application, we do not know the accurate background conductivity beneath the earth. In order to simulate this situation, in this section, it is assumed that the true background conductivity is unknown. The goal of this study is to test whether inaccurate background conductivity will affect the results of inversion for both ZTEM and AirMt data sets.

As noted above, both ZTEM and AirMt are not sensitive to variations of the 1D background conductivity, and show no response in the case of the large, horizontal 1D geoelectrical model. It is very difficult if not impossible to infer an accurate estimation of the background conductivity from ZTEM or AirMt data. In the next set of experiments, it is assumed that background resistivities differ in inversion from the true model in order to study their effect on inversion results. First we assume a more conductive background of 50 Ohm-m in the inversion compared to the true conductivity 100 Ohm-m. Figures 9 and

10 show the inversion results for the ZTEM and AirMt data, respectively. Both methods recover the shape of the anomaly well, but its depth is underestimated. There is also an apparent artifact at the bottom of the inversion domain not present in the true model. A case (not shown here) was also considered in which the background resistivity in the inversion was assumed higher than the one in the true model, which resulted in overestimation of the depth of the anomaly.

In this situation, the parameters used in the inversion are shown in Table 3.

5.3 Inversion with reference station anomaly

In this section, it is assumed that there is another conductivity anomaly located closes to the reference station. The purpose of this model study is to test whether a small anomaly under the reference position will change the results of inversion for both the ZTEM and AirMt data sets.

The inversion algorithm assumes the same 1D background model in both inversion regions as well as under the reference receiver. In the next numerical experiments, the synthetic ZTEM and AirMt data were computed assuming a 10 Ohm-m conductive anomaly $2000 \times 2000 \times 100$ m^2 100 m deep under the reference receiver. The other parameters of the model were kept constant. The data were inverted assuming no anomalies under the reference station. The results of the ZTEM and AirMt inversions are shown in Figures 11 and 12, respectively. Both inversion results recovered the L-shaped anomaly well, which indicates that conductivity variations under the reference receiver did not significantly affect the inversion results.

The parameters of the inversion are listed in Table 4.

5.4 Inversion with variable flight elevation

In this section, it is assumed that the average flight elevation is different from the one used in the forward modeling. In the numerical experiment, synthetic data were computed assuming random variations of the flight elevation within 50 m from the mean elevation of 75 m above the surface. The inversion was performed with the receiver positions at the mean elevation of 75 m. The inversion results of both the ZTEM and AirMt data recovered the anomaly well (Figures 13 and 14), indicating that quite significant variations in flight elevation could be overlooked.

The parameters of the inversion are listed in Table 5.

5.5 Inversion of the noisy data

In this numerical experiment, the inversion was applied to synthetic data contaminated with 10% noise. To simulate realistic conditions, noise was added to the magnetic field components before they were transformed into ZTEM and AirMt transform functions. Figures 15 and 16 show the inversion results of noisy ZTEM and AirMt data. The ZTEM inversion result recovers the L-shaped anomaly well, while the AirMt image is quite distorted. This indicates that the ZTEM transform was less affected by the noise in the field components. Figures 17 and 18 show observed and predicted maps of the ZTEM W_{zx} and W_{zy} components, and Figure 19 compares the observed and predicted AirMt data. It is obvious from the data maps that the AirMt amplification parameter was affected by noise much more significate then the ZTEM data.

The parameters of the inversion are listed in Table 6.

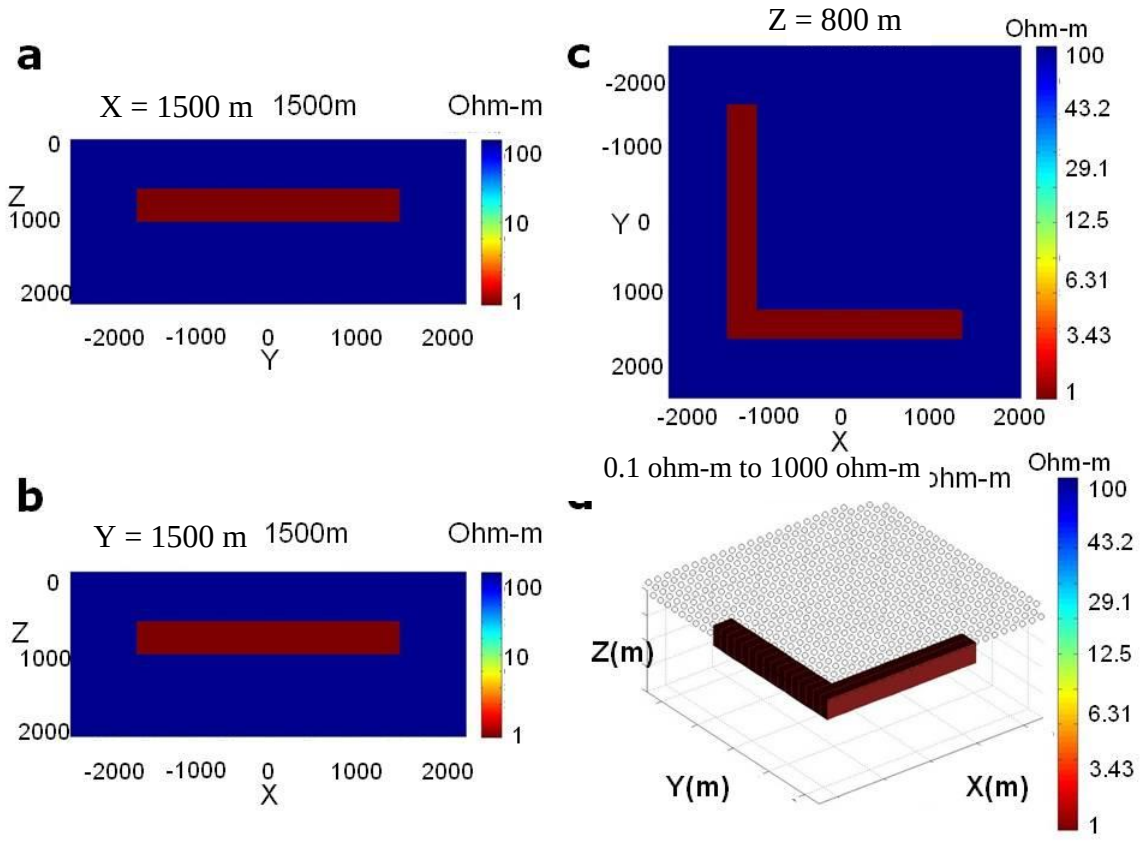

Figure 3. Basic L-shaped model: a - vertical section at X=-1500 m, b - vertical section at Y=1500 m, c - horizontal section at Z=800 m, d - 3D view of the L-shaped anomaly with receivers shown by circles.

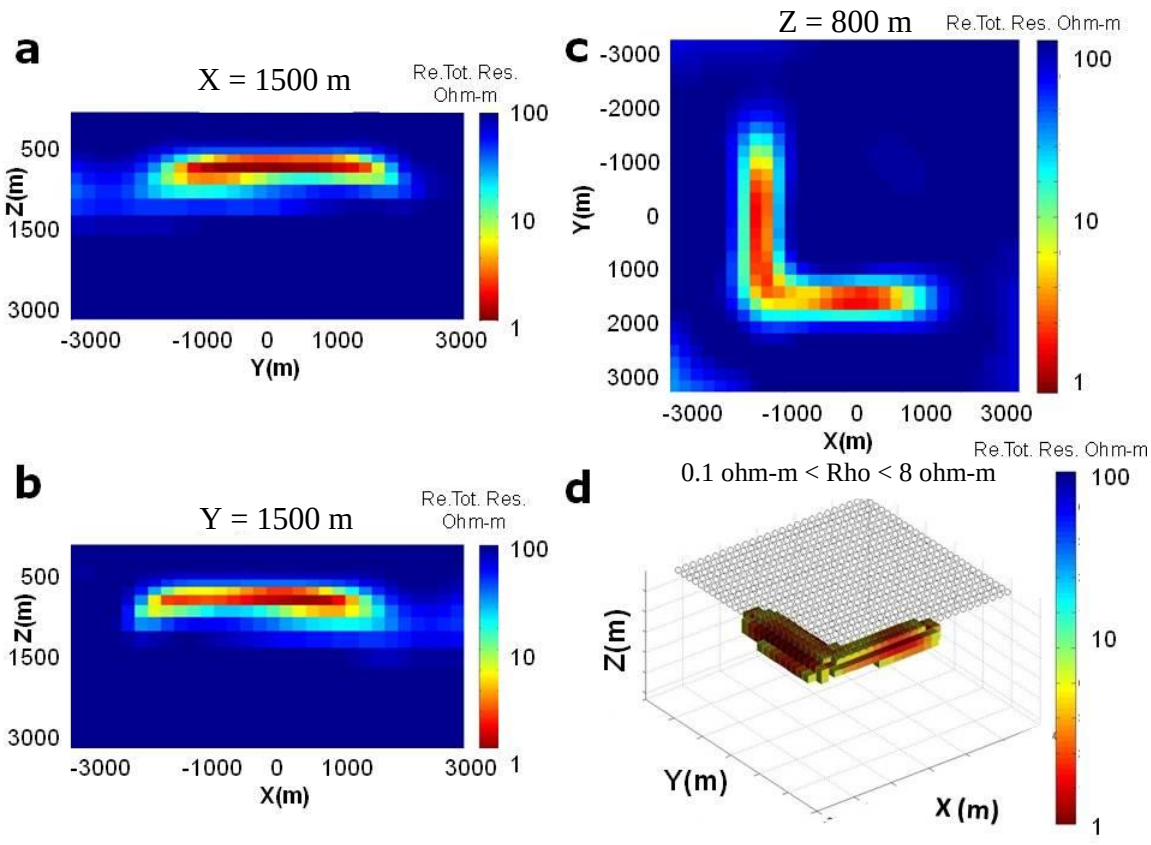

Figure 4. ZTEM inversion result with true model parameters for the L-shaped model: a - vertical section at X=-1500 m, b - vertical section at Y=1500 m, c - horizontal section at Z=800 m, d - 3D view of the predicted L-shaped anomaly with receivers shown by circles.

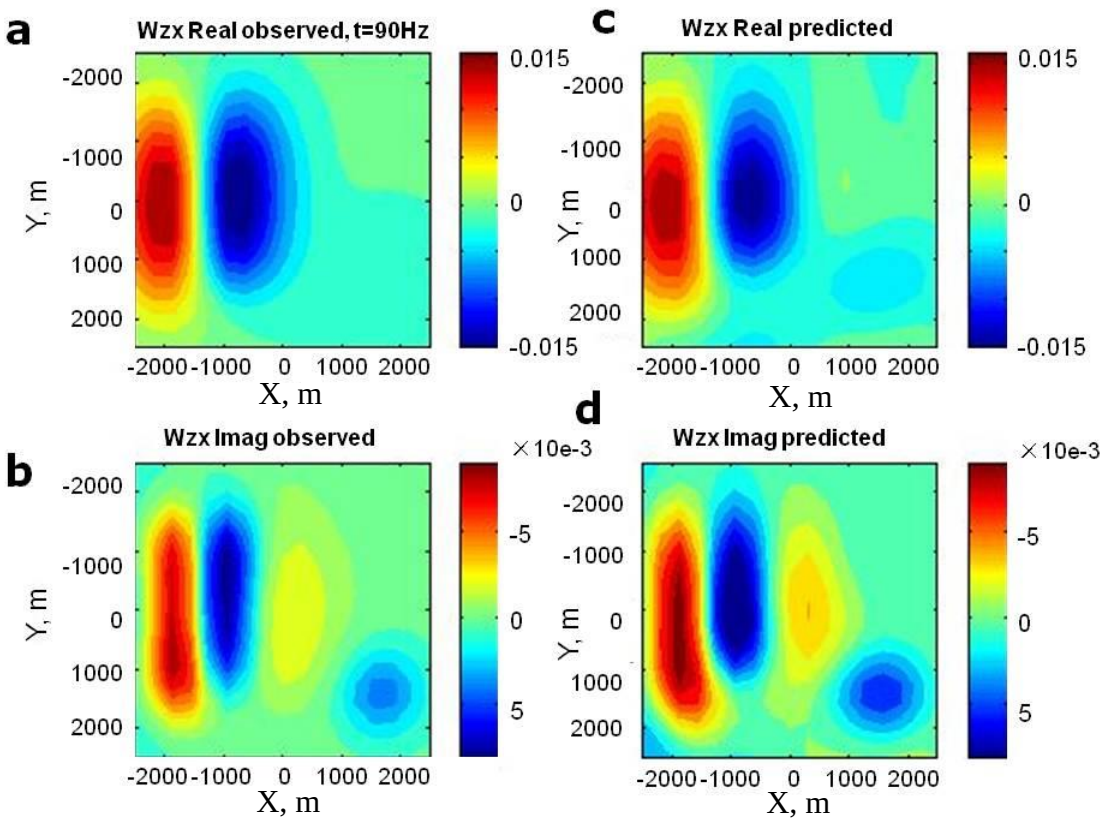

Figure 5. Maps of the observed (left) and predicted (right) real (top) and imaginary (bottom) parts of the W_{zx} ZTEM component at 90 Hz frequency.

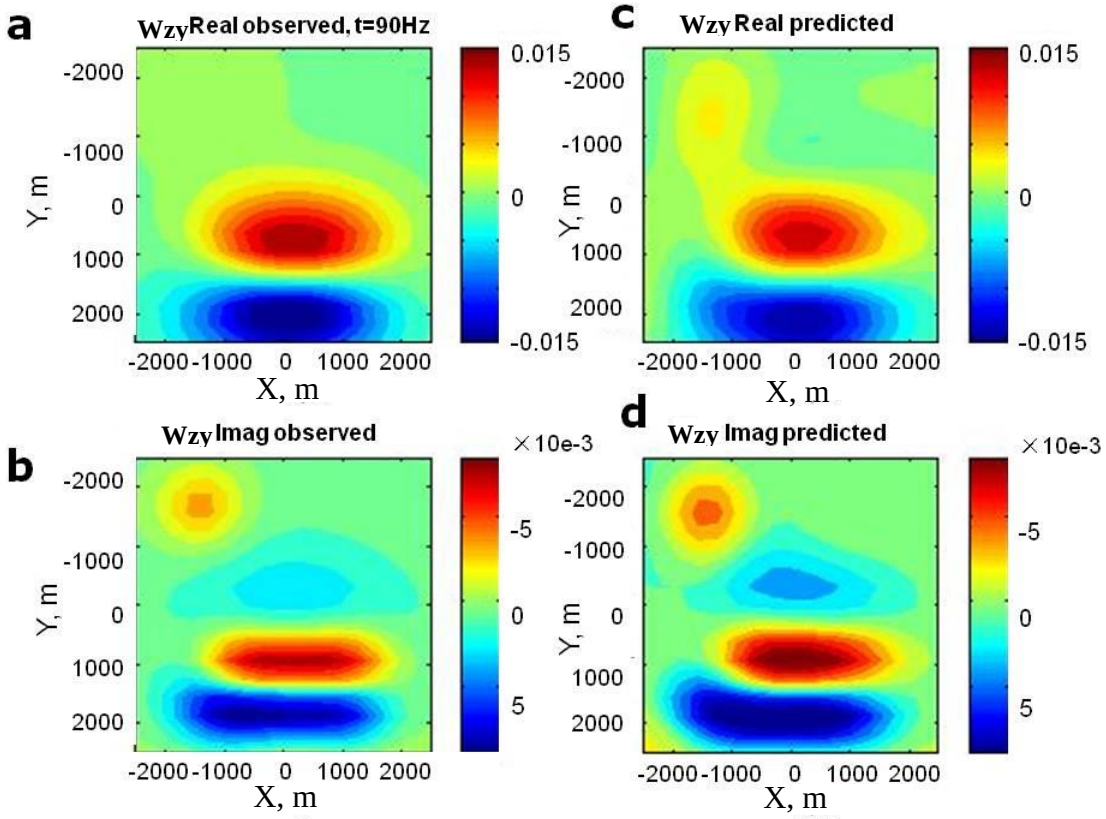

Figure 6. Maps of the observed (left) and predicted (right) real (top) and imaginary (bottom) parts of the W_{zy} ZTEM component at 90 Hz frequency.

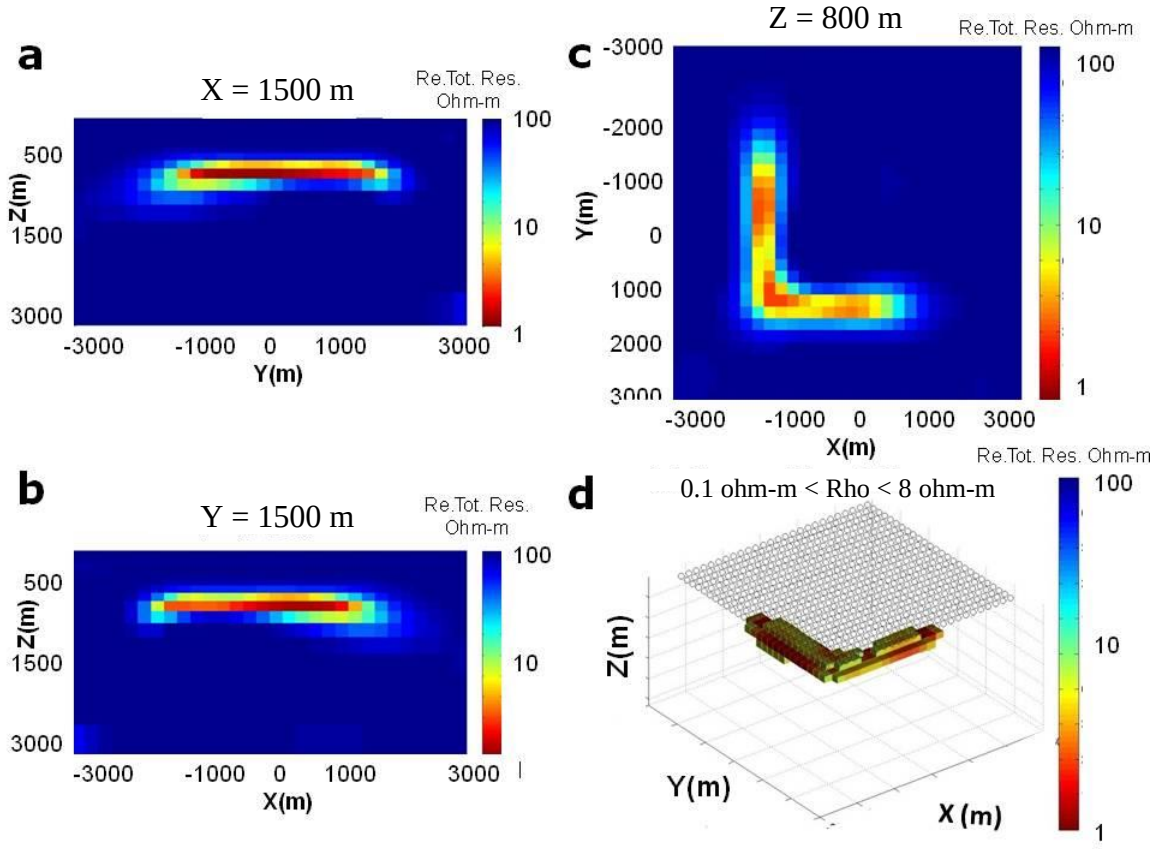

Figure 7. AirMt inversion result with true model parameters for the L-shaped model: a - vertical section at X=-1500 m, b - vertical section at Y=1500 m, c - horizontal section at Z=800 m, d - 3D view of the predicted L-shaped anomaly with receivers shown by circles.

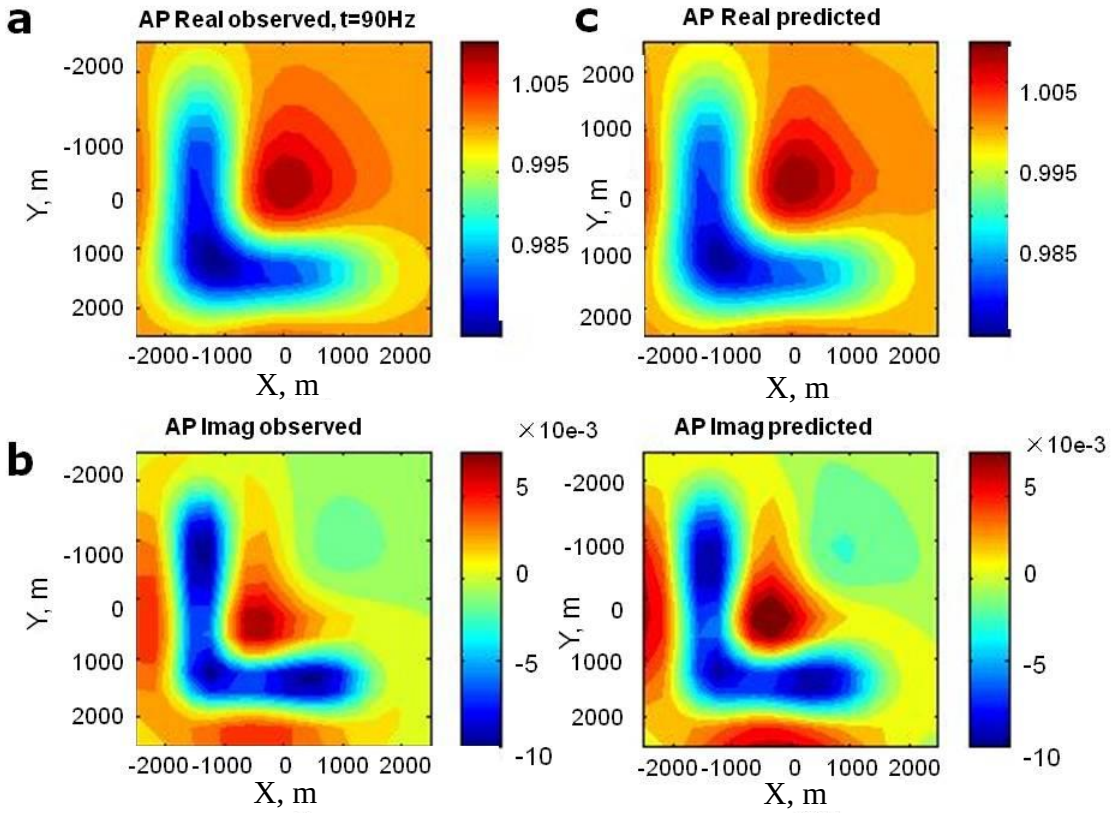

Figure 8. Maps of the observed (left) and predicted (right) real (top) and imaginary (bottom) parts of the AirMt amplification parameter at 90 Hz frequency.

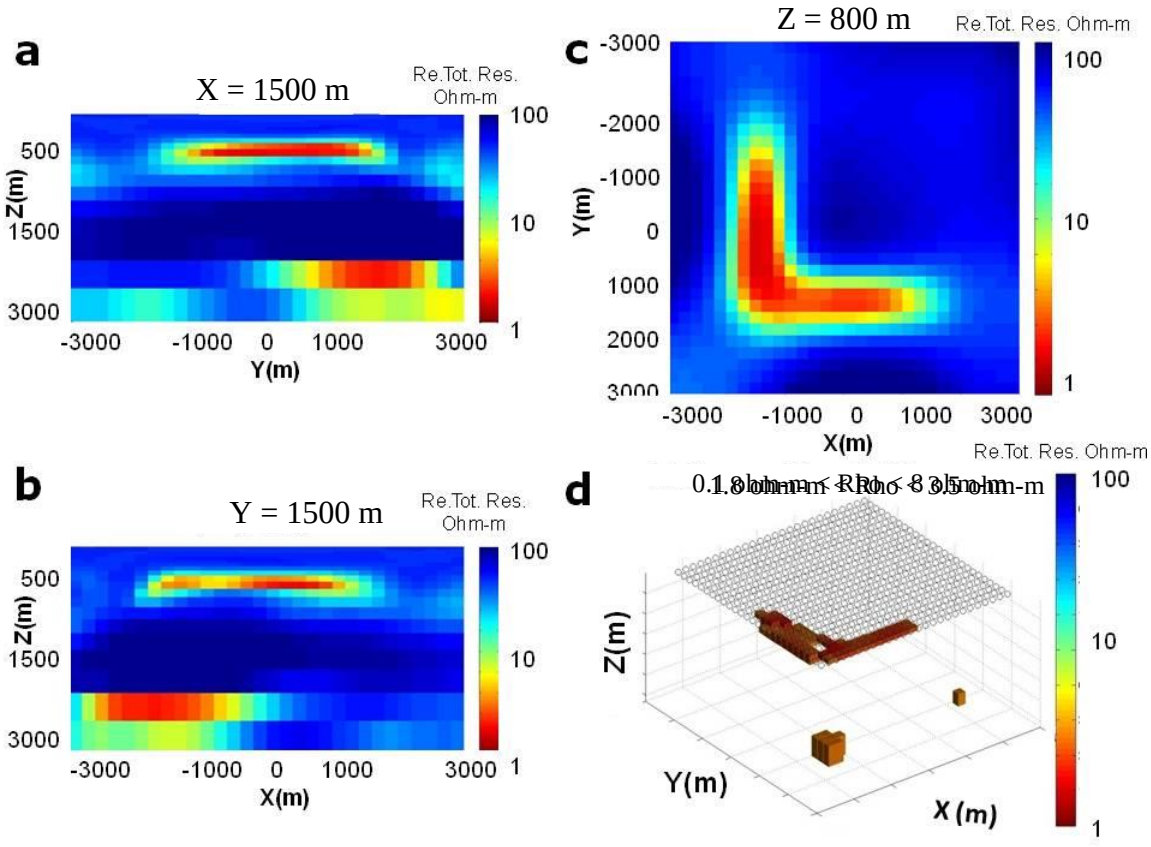

Figure 9. ZTEM inversion result with true model parameters for the L-shaped model: a - vertical section at X=-1500 m, b - vertical section at Y=1500 m, c - horizontal section at Z=800 m, d - 3D view of the predicted L-shaped anomaly with receivers shown by circles.

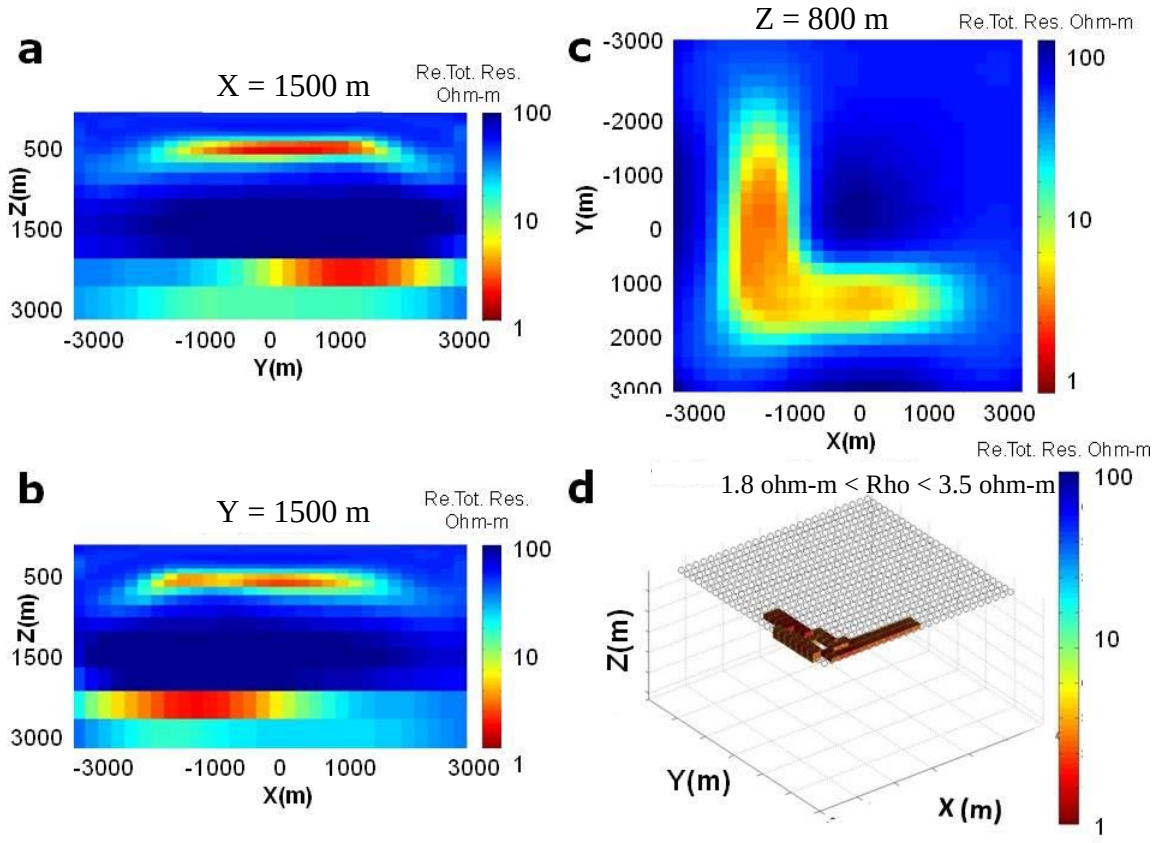

Figure 10. AirMt inversion result with true model parameters for the L-shaped model: a - vertical section at X=-1500 m, b - vertical section at Y=1500 m, c - horizontal section at Z=800 m, d - 3D view of the predicted L-shaped anomaly with receivers shown by circles.

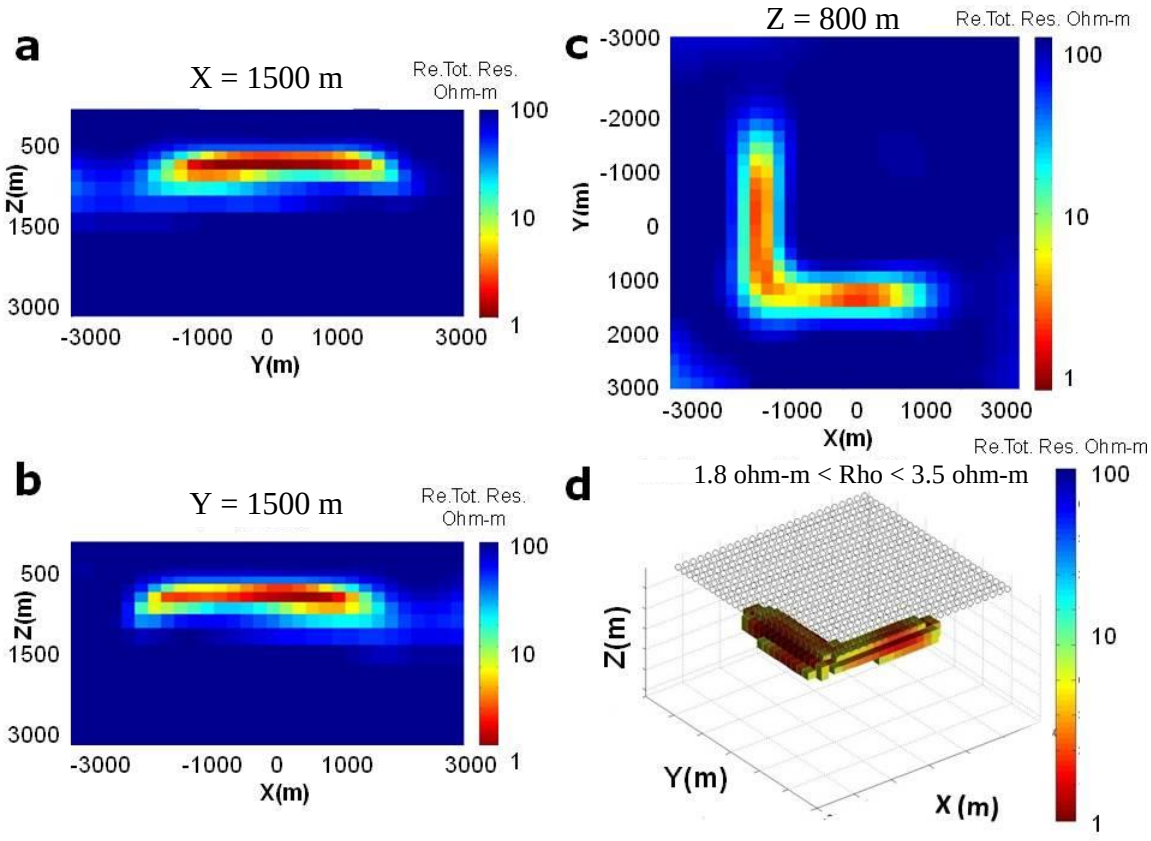

Figure 11. ZTEM inversion result with true model parameters for the L-shaped model: a - vertical section at X=-1500 m, b - vertical section at Y=1500 m, c - horizontal section at Z=800 m, d - 3D view of the predicted L-shaped anomaly with receivers shown by circles.

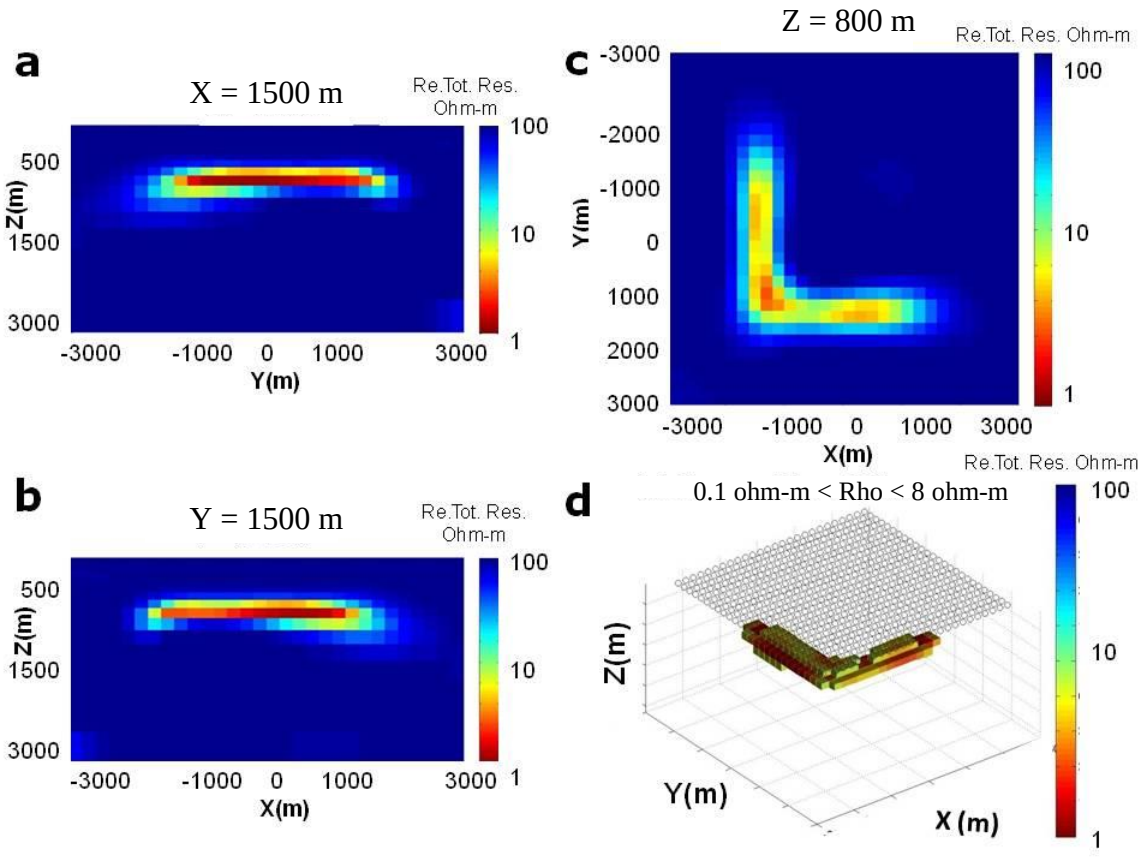

Figure 12. AirMt inversion result with true model parameters for the L-shaped model: a - vertical section at X=-1500 m, b - vertical section at Y=1500 m, c - horizontal section at Z=800 m, d - 3D view of the predicted L-shaped anomaly with receivers shown by circles.

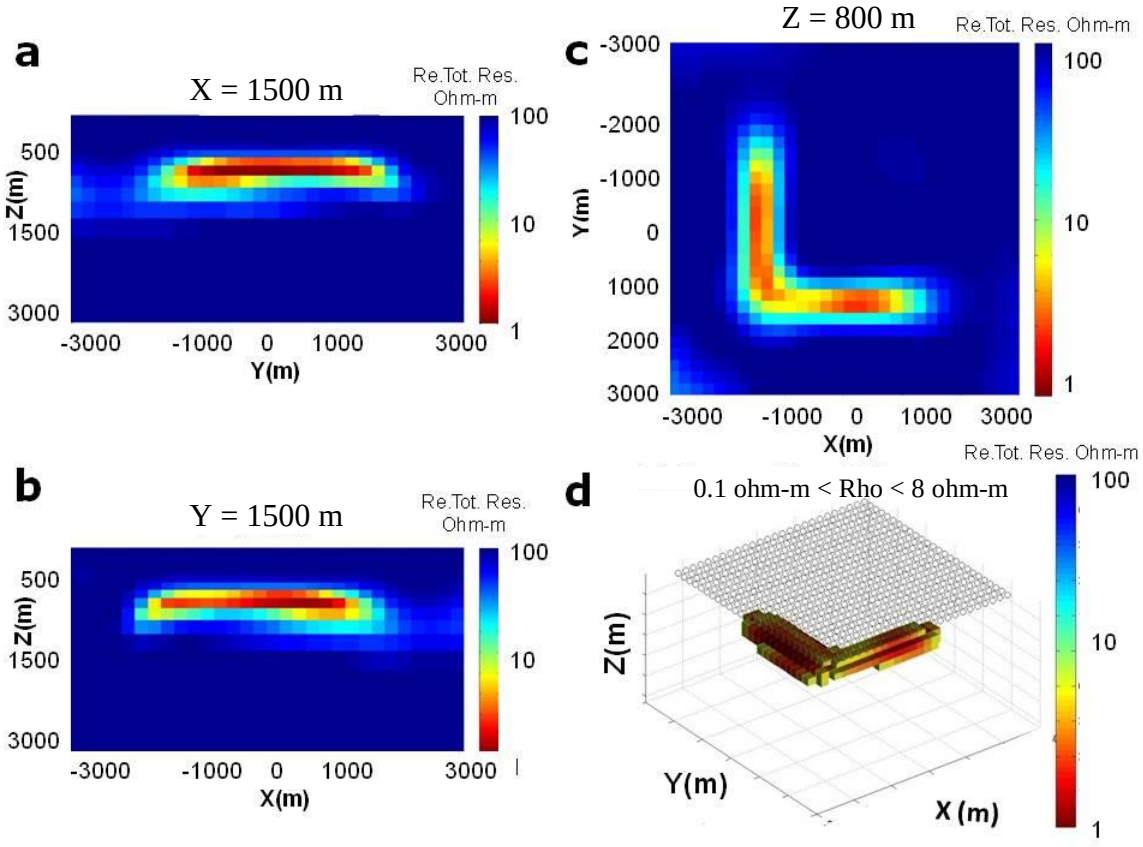

Figure 13. ZTEM inversion result with true model parameters for the L-shaped model: a - vertical section at X=-1500 m, b - vertical section at Y=1500 m, c - horizontal section at Z=800 m, d - 3D view of the predicted L-shaped anomaly with receivers shown by circles.

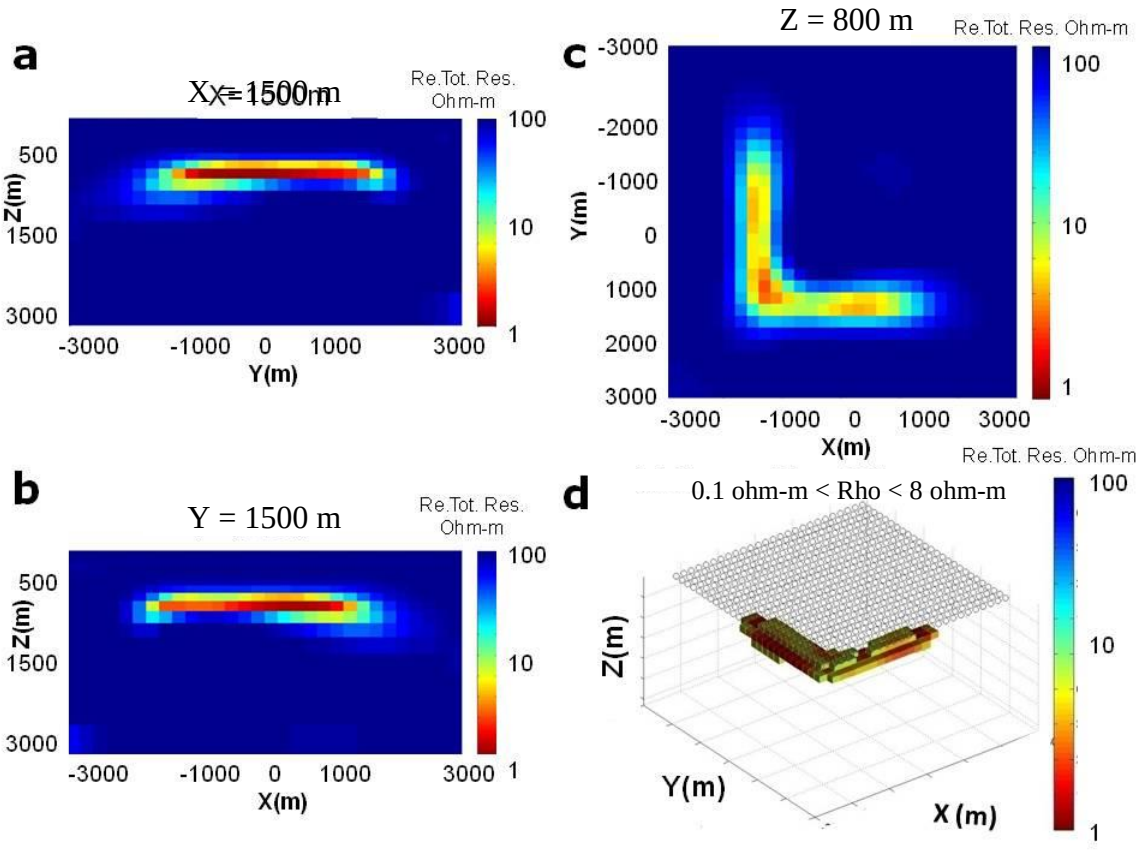

Figure 14. AirMt inversion result with true model parameters for the L-shaped model: a - vertical section at X=-1500 m, b - vertical section at Y=1500 m, c - horizontal section at Z=800 m, d - 3D view of the predicted L-shaped anomaly with receivers shown by circles.

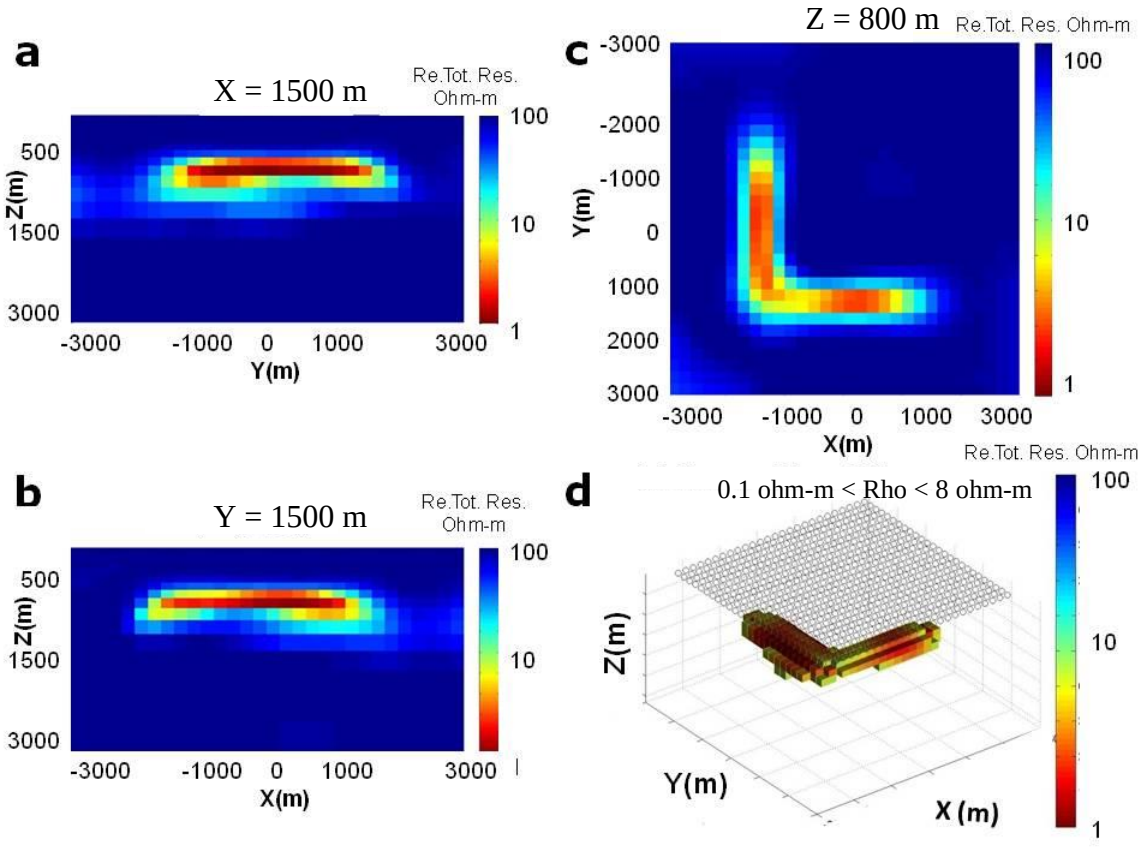

Figure 15. ZTEM inversion result with true model parameters for the L-shaped model: a - vertical section at X=-1500 m, b - vertical section at Y=1500 m, c - horizontal section at Z=800 m, d - 3D view of the predicted L-shaped anomaly with receivers shown by circles.

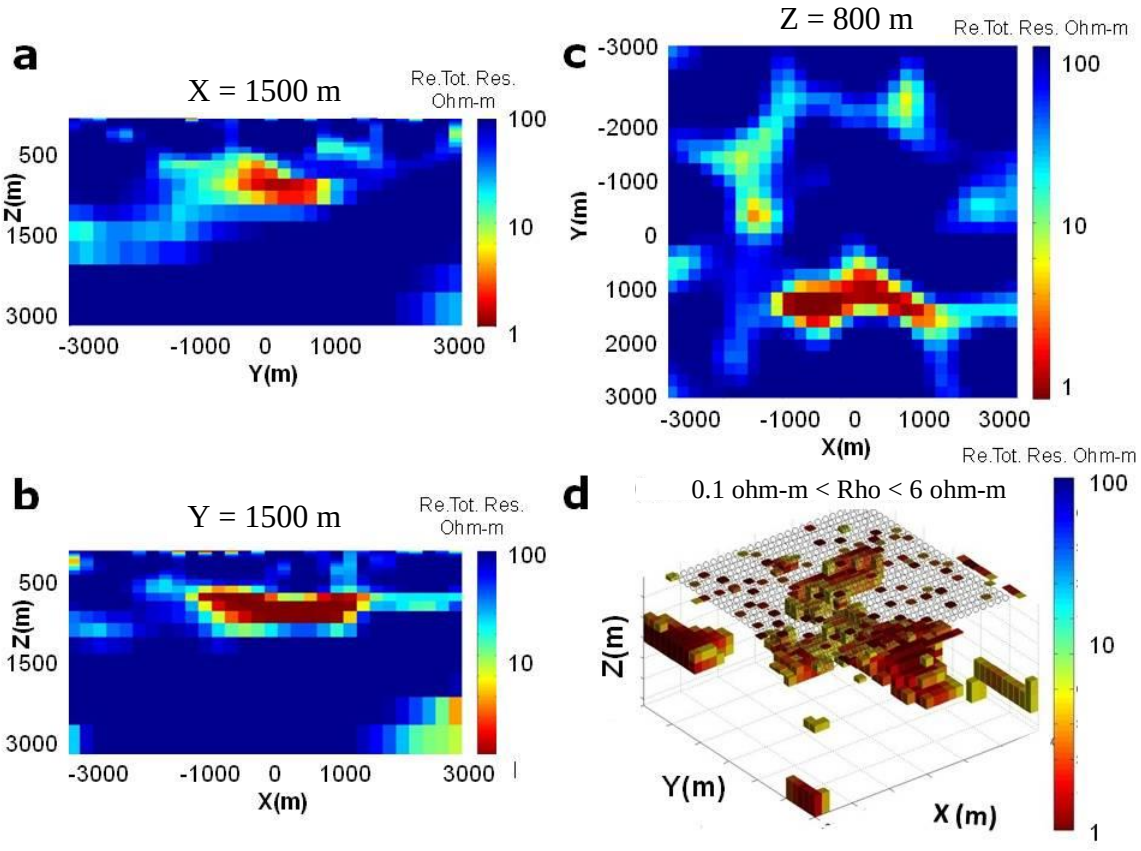

Figure 16. AirMt inversion result with true model parameters for the L-shaped model: a - vertical section at X=-1500 m, b - vertical section at Y=1500 m, c - horizontal section at Z=800 m, d - 3D view of the predicted L-shaped anomaly with receivers shown by circles.

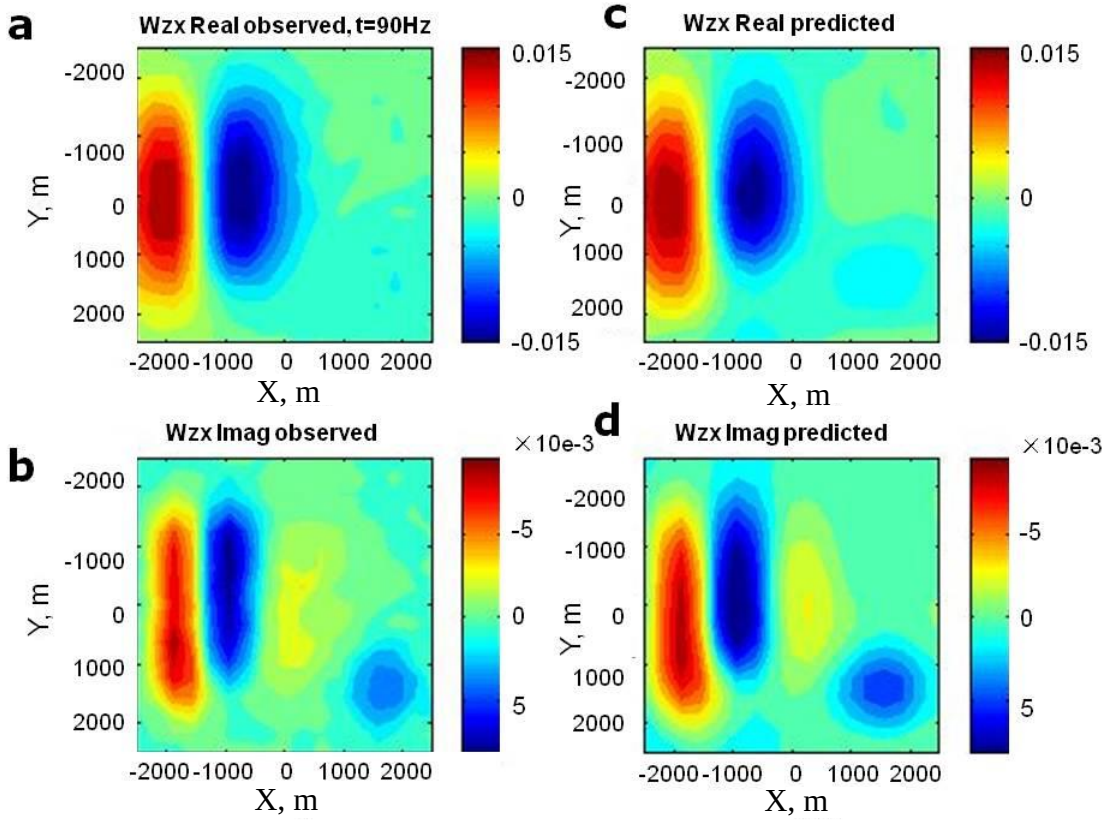

Figure 17. Maps of the observed (left) and predicted (right) real (top) and imaginary(bottom) parts of the W_{zx} ZTEM component at 90 Hz frequency.

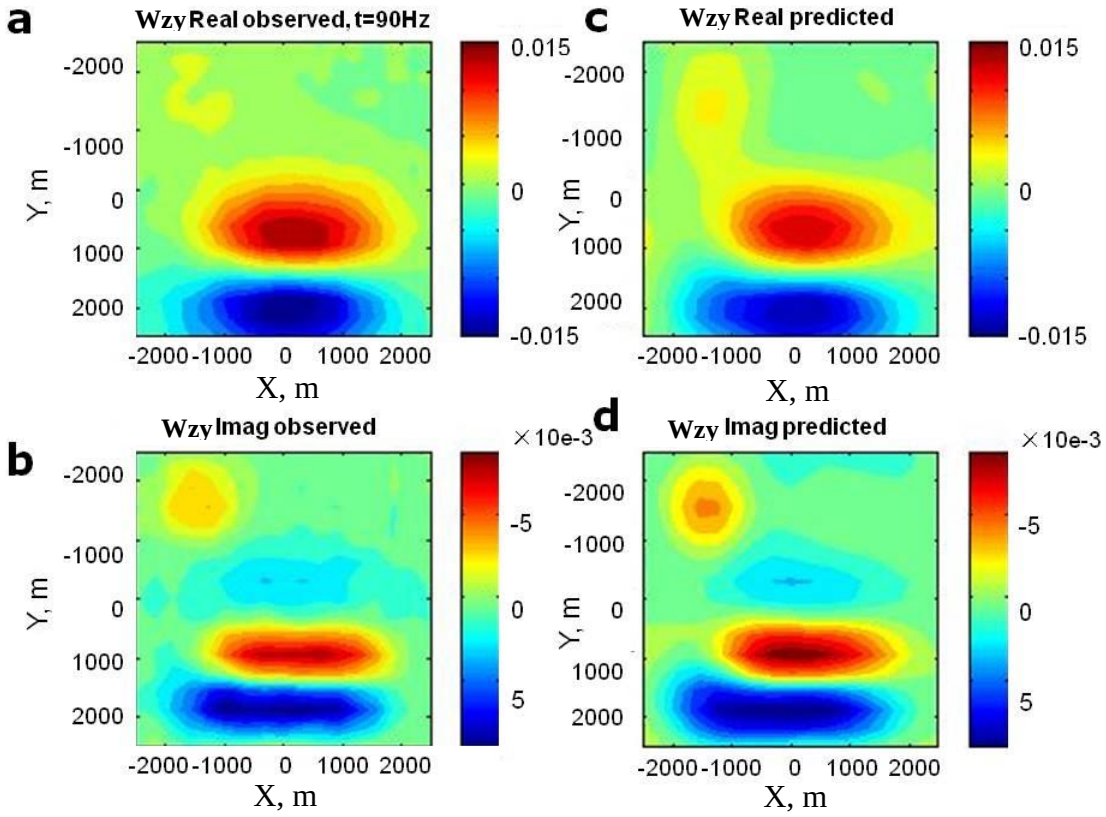

Figure 18. Maps of the observed (left) and predicted (right) real (top) and imaginary (bottom) parts of the W_{zy} ZTEM component at 90 Hz frequency.

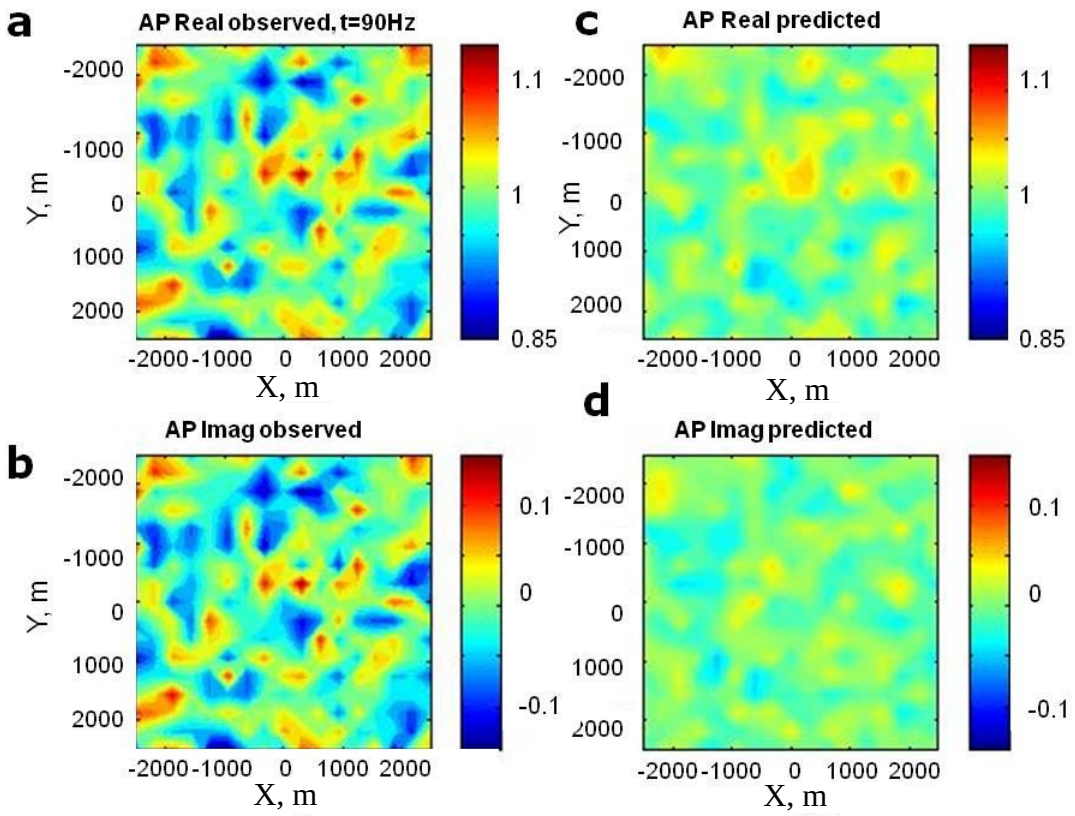

Figure 19. Maps of the observed (left) and predicted (right) real (top) and imaginary (bottom) parts of the AirMt amplification parameter at 90 Hz frequency.

Table 1 Parameters used in the basic model

Parameters	Value
ρ_b	100 Ohm-m
ρ_a	1 Ohm-m
Number of receivers	676
Elevation	75m
Frequency	[30, 45, 90, 180, 360] Hz

Table 2 Parameters used in the true model inversion parameters

Parameters	Value
Inversion domain	$6 \times 6 \times 3$ km^3
Inversion cells size	$100 \times 100 \times 50$ m^3
ρ_b	100 Ohm-m
Reference position	[10 km, 10 km, 0]
Elevation	75 m
Noise level	Without any noise

Table 3 Parameters used with inaccurate background conductivity

Parameters	Value
Inversion domain	$6 \times 6 \times 3$ km^3
Inversion cells size	$100 \times 100 \times 50$ m^3
Inversionρ_b	50 Ohm-m
Modelingρ_b	100 Ohm-m
Reference position	[10 km, 10 km, 0]
Elevation	75 m
Noise level	Without any noise

Table 4 Parameters used with reference station anomaly

Parameters	Value
Inversion domain	$6 \times 6 \times 3$ km^3
Inversion cells size	$100 \times 100 \times 50$ m^3
ρ_b	50 Ohm-m
Position of reference anomaly	[9-11 km; 9-11 km; 200-300 m]
ρ_b of new anomaly	10 Ohm-m
Reference position	[10 km, 10 km, 0]
Elevation	75 m
Noise level	Without any noise

Table 5 Parameters used with variable flight elevation

Parameters	Value
Inversion domain	$6 \times 6 \times 3$ km^3
Inversion cell size	$100 \times 100 \times 50$ m^3
ρ_b	50 Ohm-m
Reference position	[10 km, 10 km, 0]
Inversion receiver elevation	Constant at 75 m
Modeling receiver elevation	Random in 50 m within 75 m
Noise level	Without any noise

Table 6 Parameters used with variable flight elevation

Parameters	Value
Inversion domain	$6 \times 6 \times 3$ km^3
Inversion cells size	$100 \times 100 \times 50$ m^3
ρ_b	50 Ohm-m
Reference position	[10 km, 10 km, 0]
Elevation	Constant at 75 m
Noise level	With 10% random noise in field

CHAPTER 6

CASE STUDY: COCHRANE ZTEM SURVEY

6.1 Description of the survey area

On June 4th, 2011, Geotech Ltd. carried out a helicopter-borne geophysical survey over the Cochrane geophysical test site situated 20 kilometers southwest of Cochrane, Ontario.

Principal geophysical sensors included a z-axis tipper electromagnetic (ZTEM) system, and a caesium magnetometer. Ancillary equipment included a GPS navigation system and a radar altimeter. A total of 117.5 line kilometers of geophysical data were acquired during the survey.

The block is located approximately 20 kilometers southwest of Cochrane, Ontario, as shown in Figure 20.

The geology of the site is typically Archaen, with various bands of mafic to felsic metavolcanics and metasedimentary units (Figure 21). Topographically, the Cochrane survey block exhibits minimal relief with elevations ranging from 275 to 301 meters above mean sea level over an area of 22 square kilometers (Figure 22). There are some small rivers and streams found throughout the block, as well as a number of small roads. Special care is recommended in identifying any potential cultural features from other sources that might be recorded in the data.

6.2 Practical ZTEM data

The crew was based out of Cochrane, Ontario, for the acquisition phase of the survey. Survey flying was started and completed on June 4th, 2009.

The data quality control and quality assurance and preliminary data processing were carried out during the acquisition phase of the project. Final reporting, data presentation, and archiving were completed from the Aurora office of Geotech Ltd. in November, 2011.

During the survey, the helicopter was maintained at a mean height of 140 meters above the ground with a nominal survey speed of 80 km/hour for the block survey. This allowed for a nominal EM sensor terrain clearance of 70 meters and a magnetic sensor clearance of 85 meters.

The on-board operator was responsible for monitoring the system integrity. He also maintained a detailed flight log during the survey, tracking the times of the flights as well as any unusual geophysical or topographic features.

On return of the aircrew to the base camp, the survey data were transferred from a compact flash card (PCMCIA) to the data processing computer. Trained personnel then uploaded the data via ftp to the Geotech office in Aurora for daily quality assurance and quality control.

The survey was flown using a Eurocopter A-Star B2 helicopter, registration number C-GSSS.

The airborne ZTEM receiver coil measured the vertical component (Z) of the EM field. The receiver coil is a Geotech z-axis tipper (ZTEM) loop sensor which is isolated from most vibrations by a patented suspension system and is encased in a fiberglass shell. It was towed from the helicopter using an 85 meter long cable as shown in Figure 23. The

cable was also used to transmit the measured EM signals back to the data acquisition system.

The coil has a 7.4 meter diameter with an orientation to the vertical dipole. The digitizing rate of the receiver was 2000 Hz. Attitudinal positioning of the receiver coil was enabled using 3 GPS antennas mounted on the coil. The output sampling rate was 0.4 seconds.

The Geotech ZTEM base station deployed in this survey consisted of three orthogonal coils as shown in Figure 2. The field measured by these coils provided horizontal X and Y components of the EM reference field, which was further used with the airborne coil data to calculate the in-line and cross-line components of the W_{zx} and W_{zy} fields. One side of each coil was 3.04 meters.

The base station for the survey was installed near the survey block away from any cultural sources. The azimuth of the reference coil was N0$_o$ E (named as A) and for the orthogonal component it was N90$_o$ E (named as B). Angles A and B were taken into account together with azimuth of the survey lines to calculate the in-line and cross-line W_{zx} and W_{zy} fields utilizing a proprietary software.

The ZTEM data were processed using proprietary software. Processing steps consisted of the following preliminary and final processing steps:

a. Airborne EM, Mag, radar altimeter, and GPS data were first merged with EM base station data into one file.

b. Merged data were viewed and examined for consistency in an incorporated viewer.

c. In the next processing phase, the following factors were taken into account:

- The base station coils orientation with respect to the magnetic north,
- The local declination of the magnetic field,
- The suggested direction of the X-coordinate (north or line direction),
- The sensitivity coefficient that compensates for the difference in geometry between the base station and the airborne coils,
- Rejection filters for the 60 Hz and helicopter-generated frequencies.

d. Six frequencies (30, 45, 90, 180, 360, and 720 Hz) were extracted from the airborne EM time series coil response using windows of 0.4 seconds and from the base station coils using windows of 1.0 seconds.

e. The real (in-phase) and imaginary (quadrature) parts of the tipper transfer functions were derived from the in-line (X or W_{zx}) and cross-line (Y or W_{zy}) components.

f. Such processed EM data were then merged with the GPS data and magnetic base station data and exported into a Geo soft xyz file.

The next stage of the preliminary data processing was done in a Geosoft TM environment, using the following prescribed steps:

a. Import the output xyz file from the AFMAG processing, as well as the base Mag data, into one database.

b. Split lines according to the recorded line channel.

c. Perform GPS processing, flight path recovery (correcting, filtering, calculating Bird GPS coordinates, and line splitting).

d. Perform radar altimeter processing, yielding the altitude values in meters.

e. Remove magnetic spike, and filter airborne and base station data. Calculate

the base station corrected mag.

f. Apply preliminary altitude corrections to EM data (in phase and quadrature), filter and make preliminary grids and profiles of all channels.

Final data processing and quality control were undertaken by Geotech Ltd. headquarterd in Aurora, Ontario, by qualified senior data processing personnel.

A quality control step consisted of re-examining all data in order to validate the preliminary data processing and to allow for final adjustments to the data.

Altitude corrections were re-evaluated and re-applied, on component-by-component, flight-by-flight, and frequency-by-frequency bases. Any remaining line-to-line system noise was removed by applying a mild additional level correction.

6.3 Inversion results

The geophysical surveys consisted of helicopter-borne AFMAG z-axis tipper electromagnetic (ZTEM) and aeromagnetic systems using a caesium magnetometer. A total of 117.5 line kilometers of geophysical data were acquired during the survey.

In a ZTEM survey, a single vertical-dipole air-core receiver coil is flown over the survey area in a grid pattern, similar to regional airborne EM surveys. Three orthogonal-axis, air-core coils are placed close to the survey site to measure the horizontal EM reference fields. Data from the three coils are used to obtain the W_{zx} and W_{zy} tipper components at six frequencies in the 30 to 720 Hz band. The ZTEM was useful in mapping geology using resistivity contrasts, and magnetometer data provided additional information on geology using magnetic susceptibility contrasts.

For data collecting, the airborne method has 561 receivers totally, and the range is

1.29e4*7.72e3 m^2 in horizontal direction. The helicopter is around 78 m above the earth surface, and receiver is located around 76 m above the earth surface.

Before the inversion, the proper inversion parameter setting is necessary. For the inversion domain, it has 9000*3000 m^2 in the horizontal direction and around 2300m depth in the vertical direction, they have 100*100 m and increasing in log space with depth: log space (1,2.5,24), respectively. ZTEM uses 6 frequencies from 30 to 720 Hz to satisfy the sounding depth.

A significant response with respect to the felsic to intermediate metavolanic rocks responses can be observed in the ZTEM data (Figure 24). It was noted that the 3D inversion was able to fit the subtle trends on the observed ZTEM data. Figure 25 presents a horizontal cross section of the 3D resistivity at -300 m above sea level. As shown in Figure 24 and 26, the conductive features are associated with the felsic to intermediate metavolanic rocks. The actual source of this conductivity is unknown. Our future work will involve inversion of the AirMt and ZTEM data, and quantitative comparison with the ZTEM results obtained thus far.

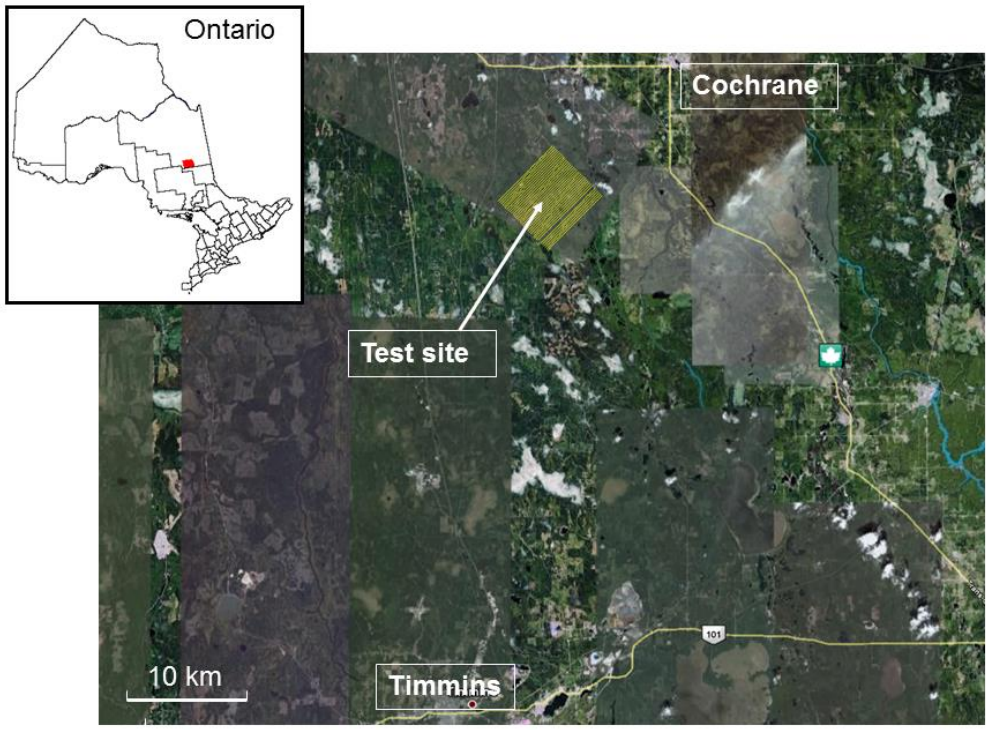

Figure 20. Location of the Cochrane test site in Ontario, Canada.

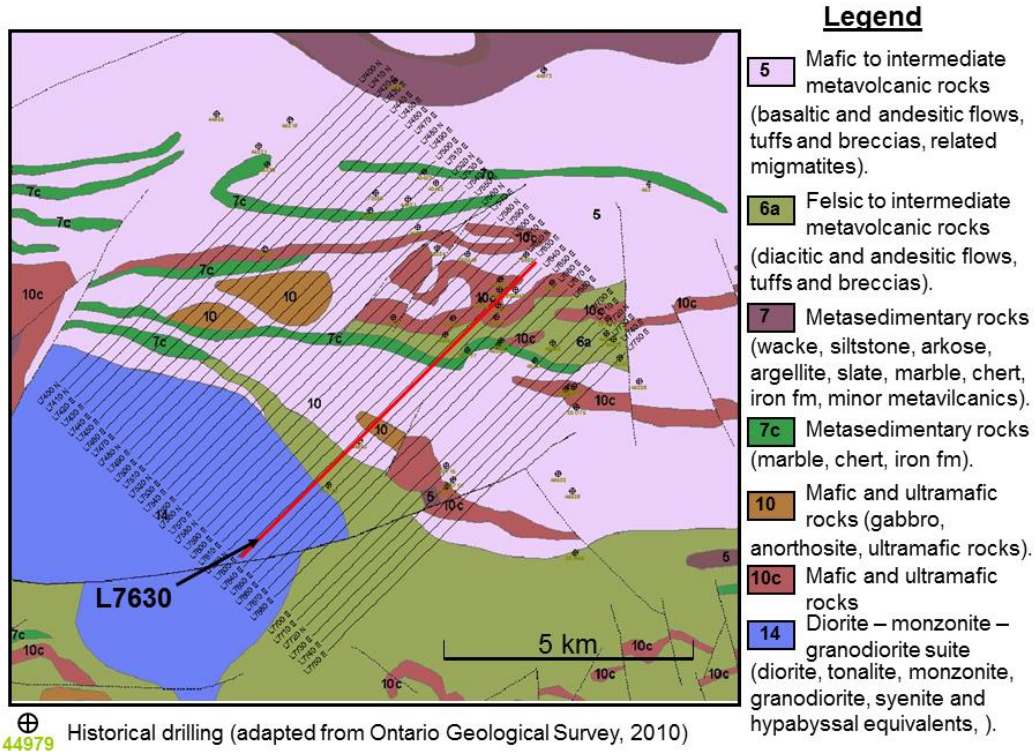

Figure 21. Geology of the Cochrane test site.

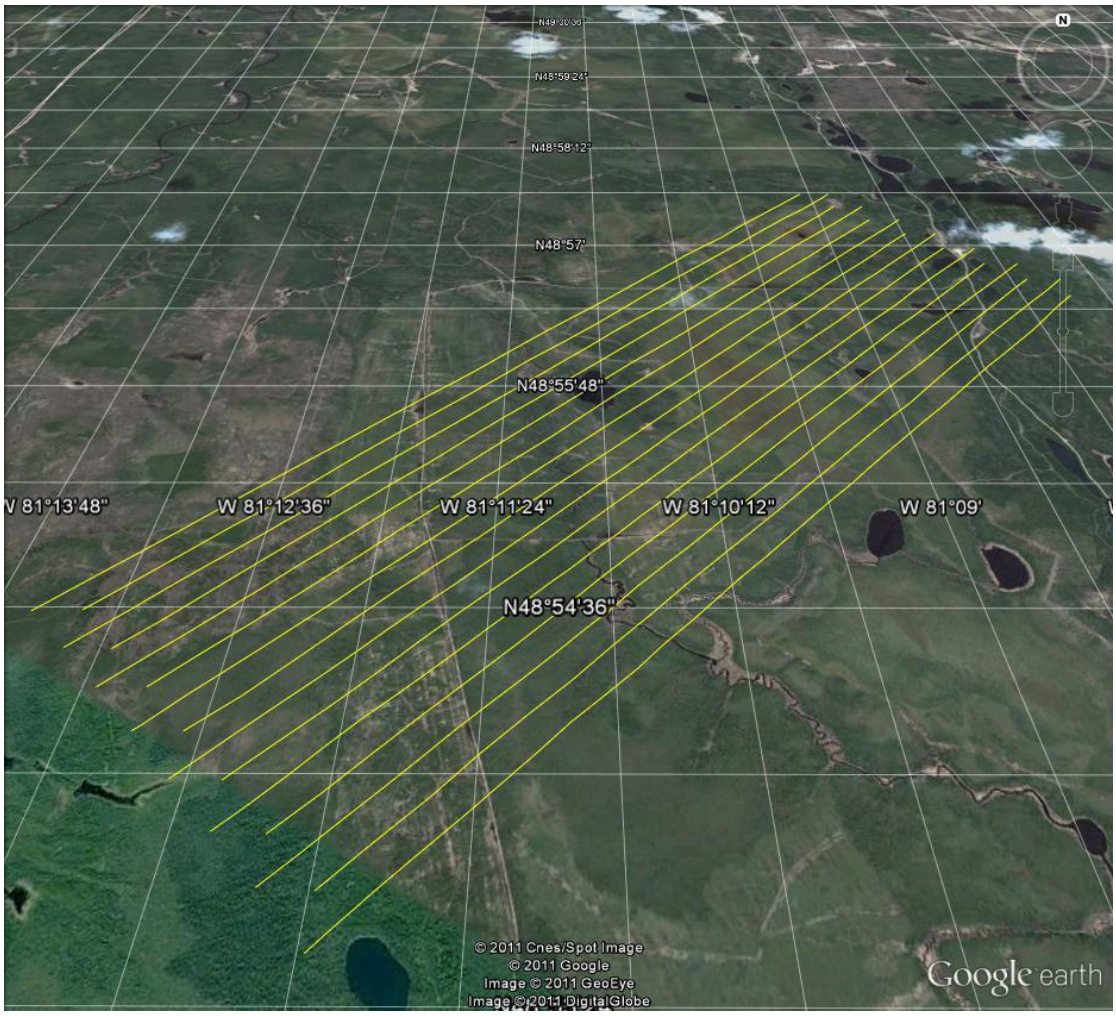

Figure 22. Google Earth image of the block.

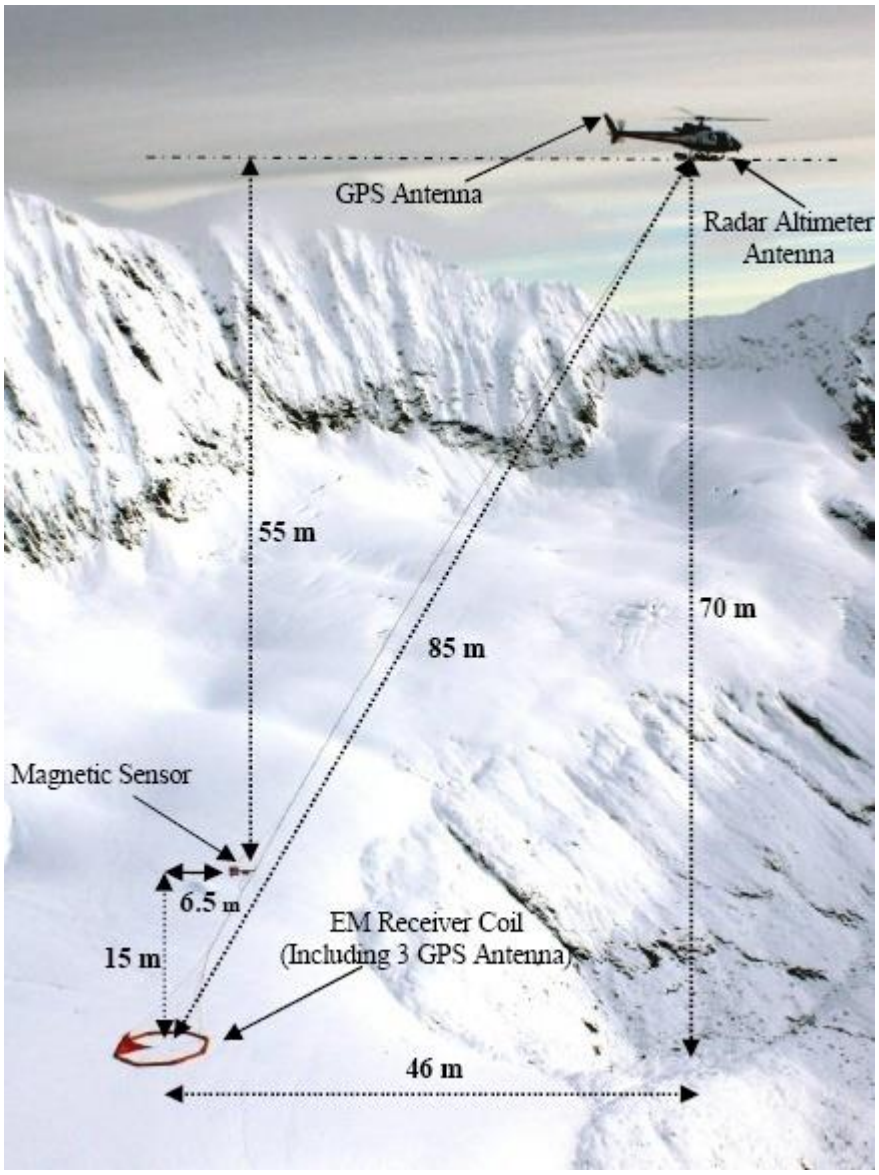

Figure 23. ZTEM system configuration.

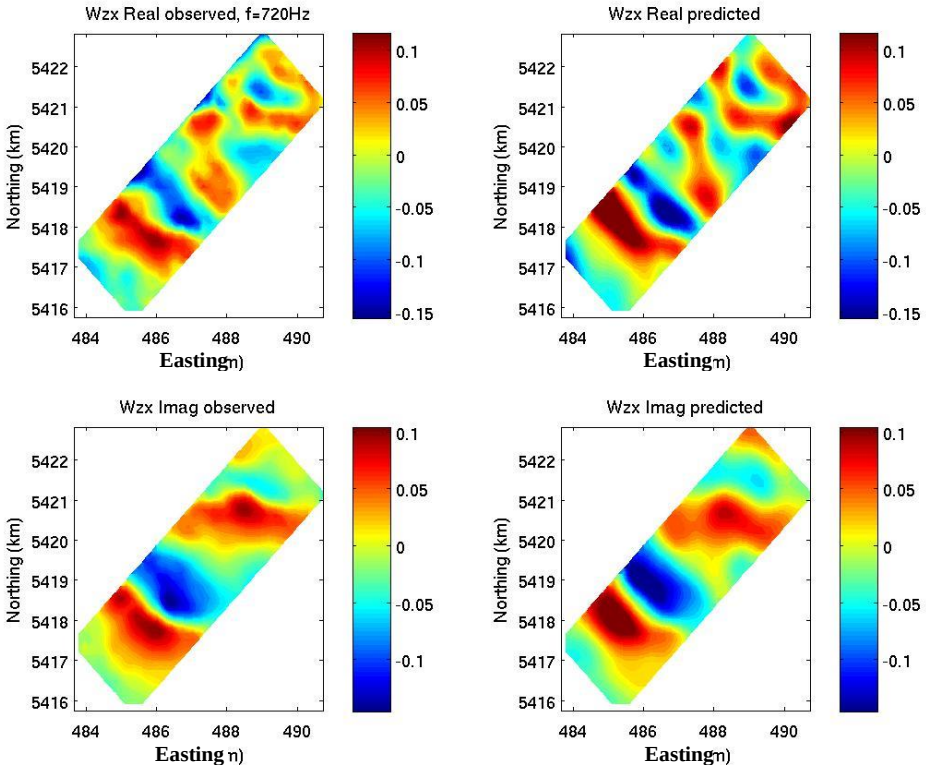

Figure 24. Observed and predicted ZTEM data for the real and imaginary components of the 720 Hz W_{zx} data.

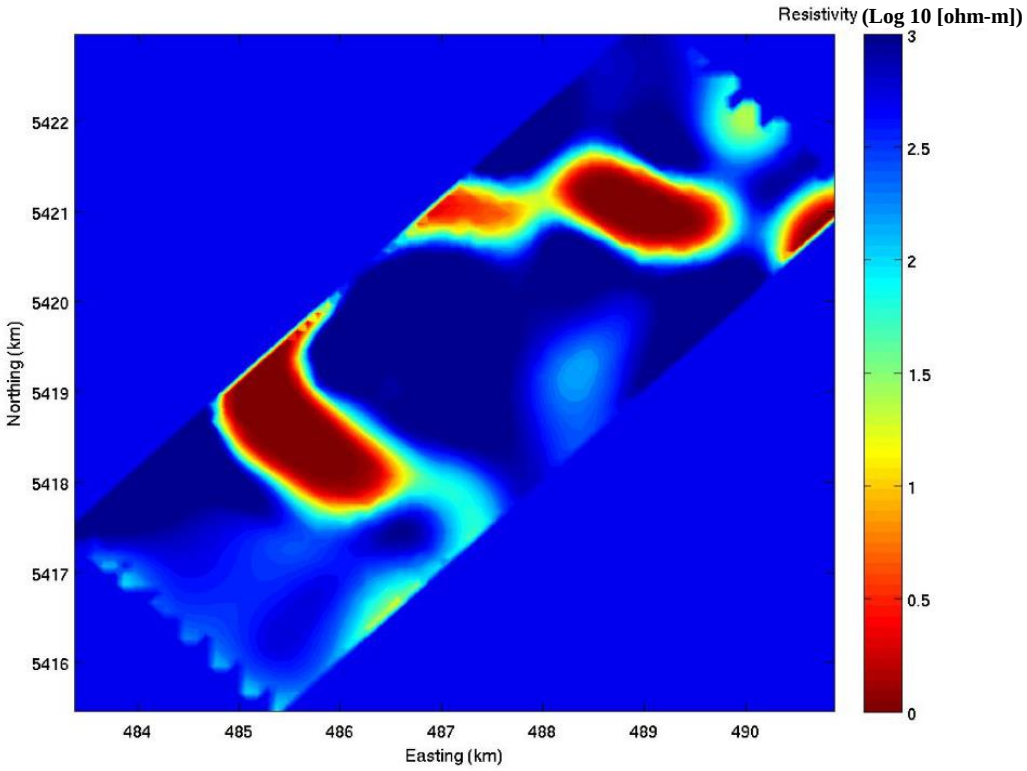

Figure 25. Horizontal cross section of the 3D resistivity model at -305 m above sea level.

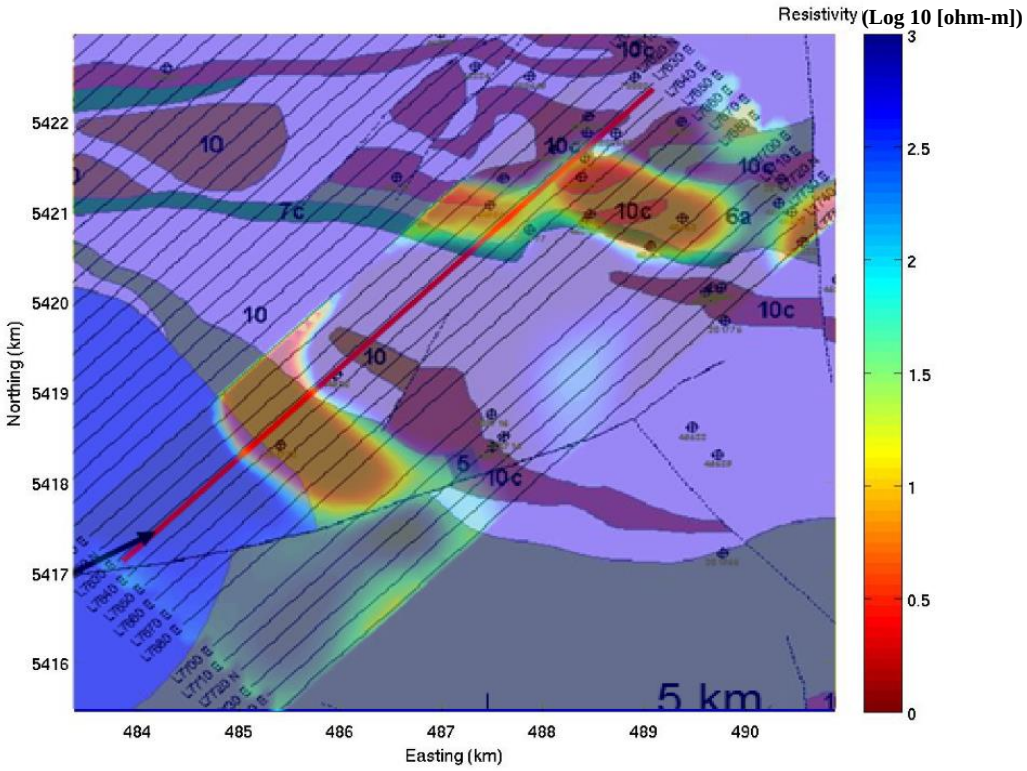

Figure 26. Horizontal cross section of the 3D resistivity model at -305 m above sea level, with the regional geology superimposed. Note the association of the conductive features with the felsic to intermediate metavolanic units.

CHAPTER 7

CONCLUSIONS

It has long been recognized that tipper data (the ratio of the local vertical magnetic field to the horizontal magnetic field) provide information about 3D electrical conductivity. However, the practical application of the tipper for airborne surveys was originated with developing the ZTEM scheme only. In ZTEM, the vertical component of the magnetic field is recorded above the entire survey area, while the horizontal fields are recorded at a ground-based reference station. The interpretation and 3D inversion of ZTEM data is still a challenge of airborne geophysics.

In this thesis, a 3D inversion algorithm using both tipper and compact amplification parameter data were introduced and applied. It is based on the nonlinear conjugate gradient algorithm and the contraction integral equation methods. To improve efficiency and reduce memory requirement, the inversion algorithm was parallelized and a receiver footprint approach was applied.

This inversion technique was first tested using synthetic data. Conductive anomalies in a half-space background were analyzed. It is shown that the inversion algorithm was able to give the accurate location and shape of the conductive anomaly. By using both the tippers and the compact amplification parameter data in the inversion, the boundaries between the anomaly and the background were well delineated. The regularized

inversions using a minimum-norm stabilizer for *the tipper* and compact amplification parameter data was also tested for different synthetic models. The inversion results yielded a predicted model with accurate conductivity contrast and a compact model shape.

The numerical model study conducted in this thesis made it possible to draw the following conclusion. Inaccurate assumptions about the background conductivity in inversion may lead to an erroneous estimation of the depths of the recovered conductivity structures. At the same time, the ZTEM data were quite stable to a significant noise level, while the AirMt data were more easily distorted, which could result in deterioration of the inverse model.

This developed 3D joint inversion algorithm was implemented for analysis of the field data in the Cochrane test site in Ontario, Canada. The inversion contained a large number of cells due to the large inversion domain and relatively fine grid. The parallelization of the code and the receiver footprint approach effectively sped up the inversion process and reduced the memory requirement. Benefitting from the application of the proper model weighting, the ZTEM inversion recovered conductive features, which, compared to those shown on a local geology map, were associated with felsic to intermediate metavolanic units.

REFERENCES

Abubakar, A., and P. M van den Berg, 2004, Iterative forward and inverse algorithms based on domain integral equations for three-dimensional electric and magnetic objects: Journal of Computational Physics, v. 195, no. 1, p. 236-262.

Alumbaugh, D., and G. Newman, 1997, Three-dimensional massively parallel electromagnetic inversion—II. Analysis of a crosswell electromagnetic experiment: Geophysical Journal International, v. 128, no. 2, p. 355-363.

Avdeev, D. B., 2005, Three-dimensional electromagnetic modelling and inversion from theory to application: Surveys in Geophysics, v. 26, no. 6, p. 767-799.

Avdeev, D. B., and A. D. Avdeeva, 2006, A rigorous three-dimensional magnetotelluric inversion: Progress in Electromagnetics Research, v. 62, p. 41-48.

Berdichevskii, M. M. N., and V. I. Dmitriev, 2008, Models and methods of magnetotellurics, Springer.

Berdichevskiĭ, M. N., and M. S. Zhdanov, 1984, Advanced theory of deep geomagnetic sounding: Elsevier Science Ltd., v. 19.

Cagniard, L., 1953, Basic theory of the magneto-telluric method of geophysical prospecting: Geophysics, v. 18, no. 3, p. 605-635.

Campbell, W. H., 2003, Introduction to geomagnetic fields: Cambridge University Press.

Cox, L. H., G. A. Wilson, and M. S. Zhdanov, 2011, 3D inversion of airborne electromagnetic data using a moving footprint: Exploration Geophysics, v. 41, no. 4, p. 250-259.

Dmitriev, V., 1969, Electromagnetic fields in inhomogeneous media: Moscow State University.

Dmitriev, V., and N. Nesmeyanova, 1992, Integral equation method in three-dimensional problems of low-frequency electrodynamics: Computational Mathematics and Modeling, v. 3, no. 3, p. 313-317.

Farquharson, C. G., D. W. Oldenburg, E. G. Haber, and R. G. Shekhtman, 2002, An

algorithm for the three-dimensional inversion of magnetotelluric data: Proceedings, SEG Annual Meeting.

Gribenko, A., A. M. Green, M. Cuma, and M. S. Zhdanov, 2010, Efficient 3D inversion of MT data using integral equations method and the receiver footprint approach: application to the large-scale inversion of the EarthScope MT data: Expanded Abstracts of the SEG meeting: Denver, Colorado, p. 644-649.

Gribenko, A., and M. S. Zhdanov, 2007, Rigorous 3D inversion of marine CSEM data based on the integral equation method: Geophysics, v. 72, no. 2, p. WA73-WA84.

Gribenko, A. V., M. S. Zhdanov, J. Legault, S. Zhao, L. H. Cox, G. A. Wilson, and K. Fisk, 2012, 3D inversion of AirMt AFMAG data: SEG Technical Program Expanded Abstracts, Society of Exploration Geophysicists, p. 1-5.

Hohmann, G. W., 1975, Three-dimensional induced polarization and electromagnetic modeling: Geophysics, v. 40, no. 2, p. 309-324.

Holtham, E., and D. W. Oldenburg, 2010, Three-dimensional inversion of ZTEM data: Geophysical Journal International, v. 182, no. 1, p. 168-182.

Kuzmin, P. V., G. Borel, E. B. Morrison, and J. Dodds, 2010, Geophysical prospectin using rotationally invariant parameters of natural electromagnetic fields, WO Patent 2,010,071,991.

Labson, V. F., A. Becker, H. Morrison, and U. Conti, 1985, Geophysical exploration with audiofrequency natural magnetic fields: Geophysics, v. 50, no. 4, p. 656-664.

Legault, J., G. A. Wilson, A. V. Gribenko, M. S. Zhdanov, S. Zhao, and K. Fisk, 2012, An overview of the ZTEM and AirMt airborne electromagnetic systems: a case study from the Nebo–Babel Ni–Cu–PGE deposit, West Musgrave, Western Australia: Preview, v. 2012, no. 158, p. 26-32.

Lo, B., and M. Zang, 2008, Numerical modeling of Z-TEM (airborne AFMAG) responses to guide exploration strategies: Proceedings, SEG Annual Meeting.

Mackie, R., and M. Watts, 2004, The use of 3D magnetotelluric inversion for exploration in complex geologic environments: Potential pitfalls and real world examples: Proceedings, AGU Fall Meeting Abstracts, Volume 1, p. 01.

Madden, T., and R. L. Mackie, 1989, Three-dimensional magnetotelluric modelling and inversion: Proceedings of the IEEE, v. 77, no. 2, p. 318-333.

Maris, V., and P. E. Wannamaker, 2010, Parallelizing a 3D finite difference MT inversion algorithm on a multicore PC using OpenMP: Computers & Geosciences, v. 36, no. 10, p. 1384-1387.

Newman, G., and D. Alumbaugh, 1997, Three-dimensional massively parallel electromagnetic inversion—I. Theory: Geophysical Journal International, v. 128, no. 2, p. 345-354.

Newman, G. A., and D. L. Alumbaugh, 2000, Three-dimensional magnetotelluric inversion using non-linear conjugate gradients: Geophysical Journal International, v. 140, no. 2, p. 410-424.

Parkinson, W., 1959, Directions of rapid geomagnetic fluctuations: Geophysical Journal International, v. 2, no. 1, p. 1-14.

Parkinson, W., 1962, The influence of continents and oceans on geomagnetic variations: Geophysical Journal of the Royal Astronomical Society, v. 6, no. 4, p. 441-449.

Raiche, A., 1974, An integral equation approach to three-dimensional modelling: Geophysical Journal International, v. 36, no. 2, p. 363-376.

Sasaki, Y., 2004, Three-dimensional inversion of static-shifted magnetotelluric data: Earth, planets and space, v. 56, no. 2, p. 239-248.

Singer, B. S., and E. Fainberg, 1997, Fast and stable method for 3-D modelling of electromagnetic field: Exploration Geophysics, v. 28, no. 2, p. 130-135.

Siripunvaraporn, W., G. Egbert, Y. Lenbury, and M. Uyeshima, 2005, Three-dimensional magnetotelluric inversion: data-space method: Physics of the Earth and Planetary Interiors, v. 150, no. 1, p. 3-14.

Stanley, S. M., 2005, Earth system history: Macmillan.

Tabarovsky, L., 1975, The method of integral equations: geoelectric applications [in Russian, Nauka, Novosibirsk, 140 pp.]

Tikhonov, A., 1950, On determining electrical characteristics of the deep layers of the earth's crust: Proceedings Sov. Math. Dokl, v. 2, p. 295-297.

Wannamaker, P. E., 1991, Advances in three-dimensional magnetotelluric modeling using integral equations: Geophysics, v. 56, no. 11, p. 1716-1728.

Wannamaker, P. E., G. W. Hohmann, and S. H. Ward, 1984, Magnetotelluric responses of three-dimensional bodies in layered earths: Geophysics, v. 49, no. 9, p. 1517-1533.

Ward, S. H., 1959, AFMAG-airborne and ground: Geophysics, v. 24, no. 4, p. 761-787.

Weidelt, P., 1975, Electromagnetic induction in three-dimensional structures: Jouranl of Geophysics, v. 41, no. 85, p. 109.

Xiong, Z., 1992, Electromagnetic modeling of 3-D structures by the method of system iteration using integral equations: Geophysics, v. 57, no. 12, p. 1556-1561.

Xiong, Z., and A. Kirsch, 1992, Three-dimensional earth conductivity inversion: Journal of computational and applied mathematics, v. 42, no. 1, p. 109-121.

Zhdanov, M., 2002, Geophysical inverse theory and regularization problems: Methods in geochemistry and geophysics: Elsevier Amsterdam.

Zhdanov, M. S., 2009, Geophysical electromagnetic theory and methods: Access online via Elsevier.

Zhdanov, M. S., and S. Fang, 1996, Quasi-linear approximation in 3-D electromagnetic modeling: Geophysics, v. 61, no. 3, p. 646-665.

Zhdanov, M. S., 1999, Three-dimensional quasi-linear electromagnetic modeling and inversion: Three-Dimensional Electromagnetics, p. 233-255.

Zhdanov, M. S., S. Fang, and G. Hursán, 2000, Electromagnetic inversion using quasi-linear approximation: Geophysics, v. 65, no. 5, p. 1501-1513.

Zhdanov, M. S., and N. Golubev, 2003, Three dimensional inversion of magnetotelluric data in complex geological structures: ASEG Extended Abstracts, v. 2003, no. 1, p. 1-39.

Zhdanov, M. S., A. Green, A. Gribenko, and M. Cuma, 2010, Large-scale three-dimensional inversion of Earthscope MT data using the integral equation method: Izvestiya, Physics of the Solid Earth, v. 46, no. 8, p. 670-678.

Zhdanov, M. S., R. B. Smith, A. Gribenko, M. Cuma, and M. Green, 2011, Three-dimensional inversion of large-scale EarthScope magnetotelluric data based on the integral equation method: Geoelectrical imaging of the Yellowstone conductive mantle plume: Geophysical Research Letters, v. 38, no. 8.

Zhdanov, M. S., and E. Tartaras, 2002, Three-dimensional inversion of multitransmitter electromagnetic data based on the localized quasi-linear approximation: Geophysical Journal International, v. 148, no. 3, p. 506-519.